3-D Shape Reconstruction of Non-Uniform Reflectance Surface Based on Pixel Intensity, Pixel Color and Camera Exposure Time Adaptive Adjustment

Jianhua Wang (wangjianhua@qut.edu.cn)
Qingdao University of Technology
Yanxi Yang
Xi'an University of Technology
Yuguo Zhou
Qingdao University of Technology

Research Article

Keywords: 3-D, pixel matching, color texture extraction, adaptive projection fringe

Posted Date: December 2nd, 2020

DOI: https://doi.org/10.21203/rs.3.rs-110986/v1

Version of Record: A version of this preprint was published at Scientific Reports on February 25th, 2021.
See the published version at https://doi.org/10.1038/s41598-021-83779-9.

3-D shape reconstruction of non-uniform reflectance surface based on pixel intensity, pixel color and camera exposure time adaptive adjustment

Jianhua Wang[1], Yanxi Yang[2] and Yuguo Zhou[1]

[1]School of Information and Control Engineering, Qingdao University of Technology, Qingdao, 266520, China

[2]School of Automation and Information Engineering, Xi'an University of Technology, Xi'an, 710048, China

[*]Corresponding Author: Jianhua Wang

Abstract: Three-dimensional (3-D) surface reconstruction of reflective objects and colored objects is a challenge. To this end, we proposed a novel approach. First, a new method of pixel matching between the projected image and the captured image is proposed. Then, we analyzed the impact of color texture and reflective surface on the captured image quality, and proposed a black-and-white (B/W) camera-based color information extraction method, an object surface reflectance and ambient light interference estimation method. Finally, the pixel color, pixel intensity and exposure time can be adaptively adjusted according to the color information and reflectivity of the measured objects. Experiments verified that the proposed method can not only obtain high-quality captured images, but also has a smaller number of additional images and a wider range of applications than existing methods.

Keyword: 3-D; pixel matching; color texture extraction; adaptive projection fringe

I. INTRODUCTION

Fringe projection profilometry (FPP) is widely used in 3-D shape reconstruction, such as reverse engineering (RE), product quality control, medical diagnosis, documentation of cultural artifacts and animation production. With the advantages of high precision, high speed, full field and non-contact, this technique has become the mainstream method in non-contact 3-D shape measurement. The reconstruction accuracy of FPP depends on the captured image quality. It is difficult to obtain high-quality images on the surface of colored objects or locally highly reflective objects, which brings great challenges to 3-D shape reconstruction of the objects with non uniform reflectivity [1-5]. Regarding the above problems, many approaches have been proposed, and these methods are generally divided into the following four categories.

(a) Methods based on multiple exposures. Zhang et al. [6] proposed a high dynamic range scanning technique based on a three-step phase shift method. By changing the aperture or exposure time, a series of fringe patterns with different brightness can be captured. Subsequently, the brightest but unsaturated pixels are extracted to form the final fringe pattern, which is used for phase calculation. Ekstrand et al. [7] proposed a technique that can automatically predict the exposure time based on the reflectivity of the object surface. This technology reduces human intervention and improves the intelligence of the 3-D shape measurement system. However, choosing a single exposure time does not always adapt to the measured surface with a wide range of reflectance changes. In addition to the method of using multiple exposure times, Liu et al. [8] also regarded the dual-camera structured light system as a two-camera-projector monocular structured light system to obtain 3-D data from different perspectives to supplement the problems caused by highlights or too dark. Jiang et al. [9] proposed a method combining bright and dark fringe projection with multiple exposures. This method reduces the influence of ambient light, improves the signal-to-noise ratio and the dynamic range of the measurement. However, since the modulation intensity of each pixel requires a square root calculation, the amount of calculation is too large. In addition, this method proposes a set of methods for automatically selecting fringe projection brightness and exposure time parameters, but the implementation process is relatively complicated. For unknown scenes, the methods mentioned above cannot directly determine the required number of exposures and the time of each exposure at the beginning of the measurement. Zhong et al. [10] also proposed an enhanced phase measurement profilometry, which selects an optimal exposure time to adapt to a wide range of surface reflectance changes. In the phase shift process, the exposure time should be as large as possible while ensuring that the image in the

strong reflection area will not be saturated. However, this method using a single exposure time is difficult to improve the signal-to-noise ratio of the stripe pattern in the weakly reflective area. Wang et al. [11] proposed an estimation algorithm for the exposure time interval. At the same time, in view of the requirements of DLP high-speed projection of binarized fringe patterns, an estimation method for the best four exposure times was introduced. The above method avoids redundant and useless multiple exposures, and can fuse the 3-D surfaces of four exposures, thereby obtaining a good 3-D shape of a non-uniform reflective surface.

(b) Polarizer-based method. For non-conductor materials, the reflected light after specular reflection is polarized, while the reflected light after diffuse reflection is not. Based on this fact, Nayar et al. [12] installed a polarizer in front of the camera and combined the color information to separate the diffuse and specular reflection areas of the image. Salahieh et al. [13] proposed a multi-polarization fringe projection system, which eliminates the image saturation point and enhances the fringe contrast by selecting an appropriate polarization channel. The projected fringe is polarized before incident on the object to be measured, and is captured by the camera after reflection. The camera is equipped with a pixel-level polarizer array with 4 states.

(c) Method based on two-color reflection model. The theoretical basis for removing highlights based on color information is the two-color reflection model proposed by Shaffer [14]. All color-based specular reflection separation methods (removing highlights) are based on the two-color reflection model. Tan et al. [15] used the information of the surrounding area of the highlight to fill the highlight area with complementary colors. Shen et al. [16] proposed a simple and effective method for separating reflection components in color images. This method is based on the error analysis of chromaticity. It selects the appropriate body chromaticity for each pixel, and uses the least square method to separate the diffuse reflection component and specular reflection component in the two-color reflection model. It does not require image segmentation or even interoperation between adjacent pixels to remove image highlights. Park and Lee [17] proposed a highlight image restoration method based on color projection. It uses two images with different exposure times to easily find the highlight area of the image. Benveniste et al. [18, 19] proposed to use color invariants to solve the problem of scanning bright surfaces under different ambient lighting, and to remove the effects of highlights. They introduced a new color invariant to detect red fringes, green fringes, and highlights, so the fringes can be stably extracted from the captured images.

(d) Methods based on the brightness adjustment of the projected fringe pattern. Kofman et al. [20, 21] found that when measured in an uncontrollable environment, changing ambient lighting will also cause the camera to saturate. They proposed a method of reducing the maximum input gray value (MIGL) to adapt to changing ambient lighting. However, for low-reflectivity surfaces, reducing the maximum input gray value will reduce the signal-to-noise ratio of the image, so it is necessary to strike a balance between image saturation and image signal-to-noise ratio. Subsequently, Kofman et al. [22, 23] proposed to project a series of fringe patterns with a decreasing maximum input gray value, and at the same time, select pixels with the largest gray value and unsaturated pixels in the phase shift image pixel by pixel to synthesize the phase shift image and use it for phase calculation. This method has a high signal-to-noise ratio for low reflectivity surface measurement, and at the same time, it can avoid image saturation for high reflectivity surface measurement, so it can obtain higher measurement accuracy. Babaie et al. [24] proposed a new method to improve the dynamic range of the fringe projection system. Based on the fringe image captured by the current camera, the image coordinates are first mapped to the projector image coordinate system, and then the pixels with saturated gray values are multiplied by masked image to reduce the brightness of the projection. The darker pixels of the fringe image are multiplied by masked image to increase the brightness until the camera can capture the fringe with high dynamic range. However, since the position of the calibration plate is not consistent with the position of the measured object, the transformation matrix and translation vector obtained by this method are not accurate enough. Zhang et al. [25] used monochrome black and white fringe patterns to measure objects with different reflectances, thereby improving robustness. They used an adaptive intensity mask to dynamically adjust the pattern intensity to prevent overexposure of bright areas. This Coded mask is derived from point spread function and camera response function. Compared with traditional methods, this method usually requires 3 iterations to quickly find the point spread Function. The point spread function is based on the homography matrix between the camera image plane and the projector image plane, which can be obtained by the advanced measurement platform calibration. However, it is difficult to ensure the position of the measured object during measurement and the position of the calibration board is completely consistent, so the coordinates after the homography matrix mapping are not very accurate.

In this paper, we first proposed a novel pixel matching method, which established the pixel matching between the projected image and the captured image. Then, we proposed a B/W camera-based color information extraction method, an object surface reflectance and ambient light interference estimation method. Finally, the pixel color, pixel intensity and exposure time can be adaptively adjusted according to the color information and reflectivity of the measured objects.

II. Principle of the Proposed Method

A. Establish the pixel relationship between the captured and projected images

As shown in Fig. 1, the computer generates a fringe pattern and projects it onto the screen. The size and relative position between the camera's field of view and the projector's field of view depends on the measurement system. When the projector, camera and object distance on the measurement system are determined, the size and relative position of the camera's field of view and the projector's field of view will also be determined. For point *A* on the object, it corresponds to the pixel position $P_P(u_P, v_P)$ of the projected image and the pixel position $P_C(u_C, v_C)$ of the captured image. In this work, we proposed a method to establish the pixel relationship between the captured and projected images. That is, for each pixel on the captured image, you can find the corresponding pixel on the projected image [26]. If the pixel relationship is established, for 3-D measurement of colored objects, objects with large-range reflectance changes, etc., the color and intensity of the corresponding pixels on the projected image can be adjusted according to the color and intensity of the captured image, thereby improving the accuracy of the 3-D measurement.

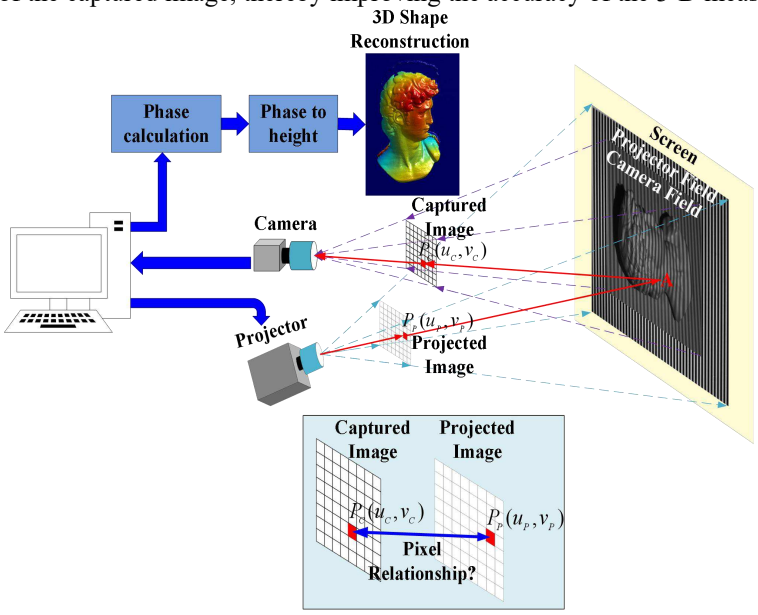

Fig. 1. Camera and projector field of view.

1) Rough coding of the entire projection pattern based on Gray coding

As shown in Fig. 2, 8 row Gray coded patterns and 8 column Gray coded patterns are sequentially projected. Therefore, the row coding of the entire projected image is 0000 0000~1000 0000, and the column coding is also 0000 0000~1000 0000. That is, the row and column of the projected image are divided into 256. However, the size of our projected image is 1024*1024 pixels, so the 4*4 matrix pixels on the projected image will correspond to the same row number and column number. If we encode each pixel on the projected image, the intensity change of a pixel of the projected image is difficult to distinguish on the captured image, while the intensity change of the 4*4 matrix pixels can be distinguished by the camera.

The camera captures 8 row-encoded images and 8 column-encoded images, respectively. Then the row and column codes corresponding to each pixel of the camera image can be calculated. However, the 4*4 rectangular pixels of the projector image have the same row and column codes. Therefore, the pixel matching between the camera's image and the projector's image is called rough matching. Obviously, the above pixel coding and matching are not accurate. For example, a certain pixel on the camera's image may correspond to multiple pixels on the projected image. Therefore, we will propose a fine coding and matching method in the next section.

2) Fine matching based on pixel shifting

Fine Gray code of the row is shown in Fig. 3. Since the fine Gray code of the column is similar, it is omitted here. The algorithm flow of fine matching is as follows.

Step 1: We project Gray coded images in sequence and capture them by a camera. We assume that the coordinate of one pixel of the camera image is (u_C, v_C), its corresponding Gray code (M_G, N_G) can be obtained by the method in Fig. 2. M_G is the row Gray code and N_G is the column Gray code [27, 31]. The coordinate on the projected image corresponding to (M_G, N_G) is (M_1, N_1).

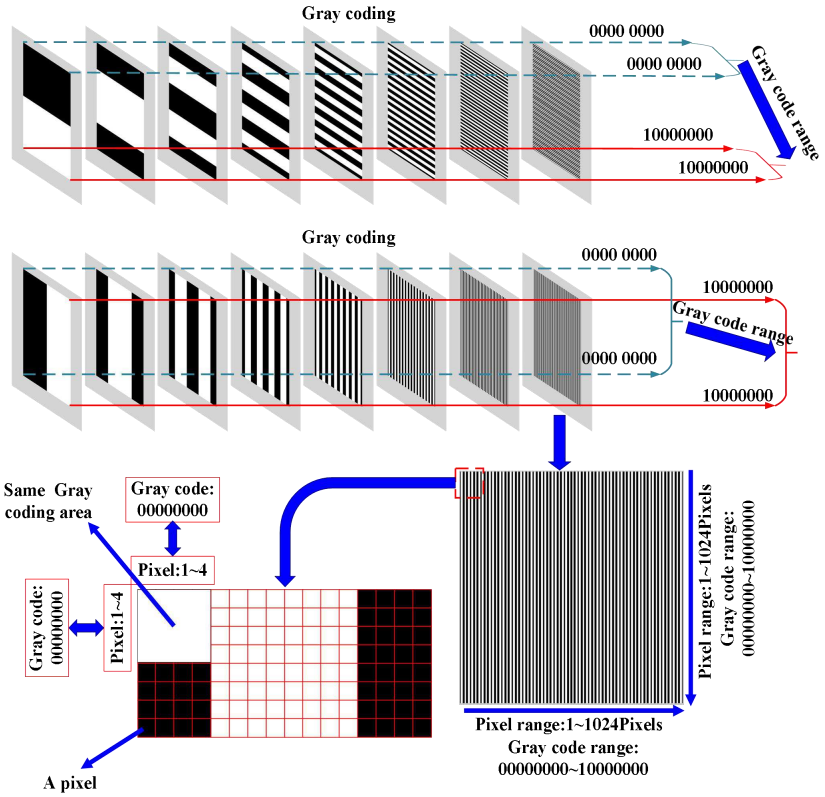

Fig.2. Rough coding of the entire projection pattern based on Gray coding.

Step 2: As shown in Fig. 3, we cycle the Gray coded images one row, and then project and capture the images. If the coordinate on the projected image is not (M_1, N_1), we can determine that the fine coordinate of the pixel on the projected image corresponding to (u_c, v_c) is (4*(M-1)+1, 4*(N-1)+1). If the coordinate on the projected image is still (M_1, N_1), then we enter the third step.

Step 3: Again, we cycle the Gray coded images one row, and then project and capture the images. If the coordinate on the projected image is not (M_1, N_1), we can determine that the fine coordinate of the pixel on the projected image corresponding to (u_c, v_c) is (4*(M-1)+2, 4*(N-1)+2). If the coordinate on the projected image is still (M_1, N_1), then we enter the fourth step.

Step 4: We recycle the Gray coded images one row, and then project and capture the images. If the coordinate on the projected image is not (M_1, N_1), we can determine that the fine coordinate of the pixel on the projected image corresponding to (u_c, v_c) is (4*(M-1)+3, 4*(N-1)+3). If the coordinate on the projected image is still (M_1, N_1), we can determine that the fine coordinate of the pixel on the projected image corresponding to (u_c, v_c) is (4*(M-1)+4, 4*(N-1)+4).

According the above method, we can establish the pixel relationship between the captured and projected images.

B. Use the B/W camera to capture the color texture

There is a problem of information crosstalk between the information components of each channel of a color camera. Therefore, a B/W camera is usually used to capture the fringe pattern. We give a simple approach for extracting the color textures based on a B/W camera.

Colorful objects can be seen everywhere. All the colors can be synthesized from three primary colors (Red, Green and Blue, i. e. RGB) in different proportion. Additive method of three primary colors is shown in Fig. 4(a). We project RGB light onto the whiteboard and use a B/W camera to capture the images. The color of whiteboard can be synthesized from the captured images.

$$I^{Color}(x,y) = cat(3, I^{Red}(x,y), I^{Green}(x,y), I^{Blue}(x,y)), \tag{1}$$

where I^{Color} represents the color of the measured object, I^{Red}, I^{Greeb} and I^{Blue} represent the grayscale captured by a B/W camera when RGB light is projected, *cat* is a operator to concatenate arrays along specified dimension.

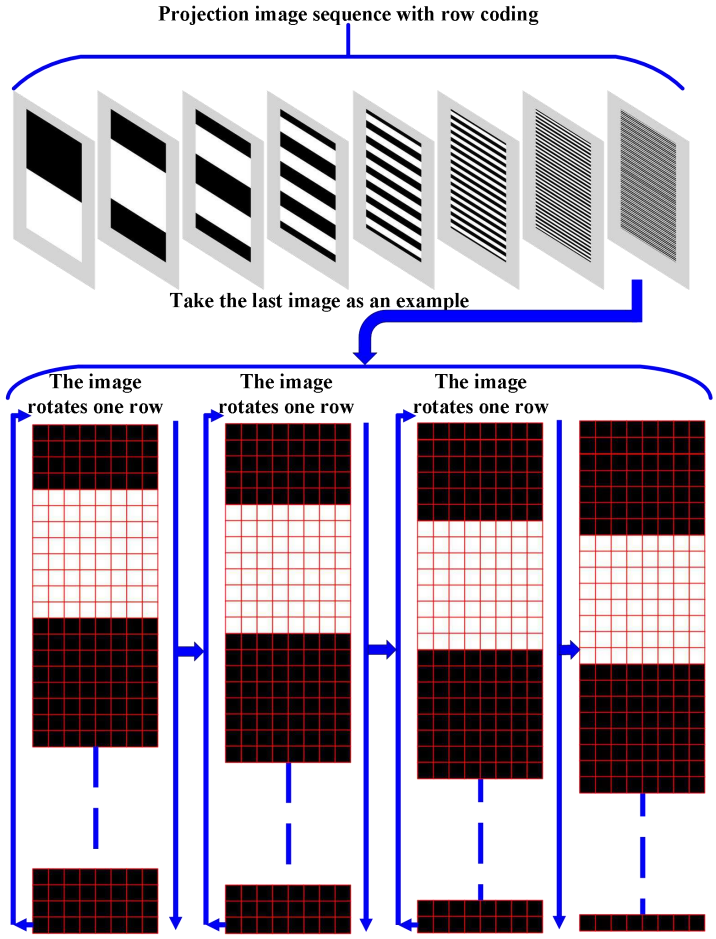

Fig. 3. Fine coding of row.

Figure 4(b) show the intensity of a line of pixels of the captured images. It can be seen from Fig. 4(b) that the intensity of the captured images is different. However, for the whiteboard, the intensity of the captured images should be equal to get white texture correctly, so we must make necessary adjustment to ensure that the grayscale of the three images is close to each other.

The intensity of the projected image is constant, the intensity of the captured image is determined by the camera's sensitivity. The camera sensitivity can be expressed as

$$C_S = f(C_A, C_T), \tag{2}$$

where C_S represents the camera sensitivity, C_A represents the aperture of camera lens, C_T is the camera exposure time.

The projected fringe pattern employing phase-shifting (PS) algorithm can be expressed as

$$I_P^n(x_P, y_P) = A(x_P, y_P) + B(x_P, y_P)\cos[\varphi(x_P, y_P) + 2\pi(n-1)/N], \tag{3}$$

where I_P^n represents the intensity of the nth projected fringe pattern, (x_P, y_P) is the coordinate of a pixel on the projected image, A is the average intensity of the projected fringe pattern, B is the modulation intensity of the projected fringe pattern, n represents the nth phase shifting, N represents the total number of phase shifting.

The captured fringe pattern can be expressed as

$$I_C^n(x_C, y_C) = C_S\left[r(x_C, y_C)I_P^n(x_P, y_P) + A_L(x_C, y_C)\right], \tag{4}$$

where I_C^n represents the intensity of the nth captured fringe pattern, r represents the reflectivity of the object surface, A_L represents the ambient light.

Parameters r and I_P^n are constant. Since adjusting the aperture of camera lens is not automatic and quantitative, adjusting the camera's exposure time is adopted in this work. The captured fringe pattern can be rewritten as

$$I_C^n(x_C, y_C) = C_T\left[r(x_C, y_C)I_P^n(x_P, y_P) + A_L(x_C, y_C)\right], \tag{5}$$

where T^C is the camera's exposure time.

Figures 5 show the camera characteristics at different exposure time. Gray value is obtained by calculating the average value of the whole image. It can be seen that the camera characteristic is approximately first-order linear on the

premise that the exposure time is not too high and the captured image is not overexposed. In order to eliminate the non-linear segment and overexposure segment, we choose the exposure time interval of 60-100 for fitting. This is reasonable because the fringe images captured in 3-D measurement cannot be overexposed as well.

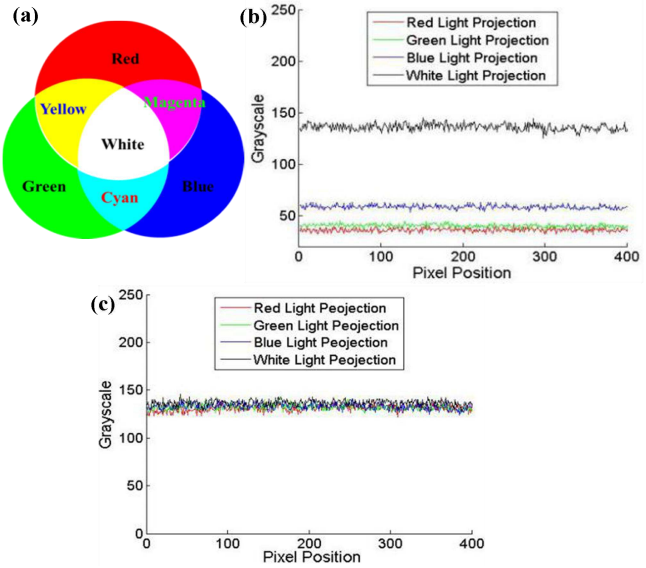

Fig. 4. The principle of color texture extraction using B/W camera. (a) Additive method of three primary colors. (b) The intensity of the captured images employing white, red, green and blue light projection. (c) The intensity of the captured images after the exposure time adjustment.

$$\begin{cases} I^R = 2.2849C_T - 7.8197 \\ I^G = 0.7739C_T - 9.3427 \\ I^B = 1.0518C_T - 8.5738 \\ I^W = 0.712C_T - 6.9571 \end{cases}, \tag{6}$$

where I^R, I^G, I^B and I^W represent the average gray value when RGB and white light are projected.

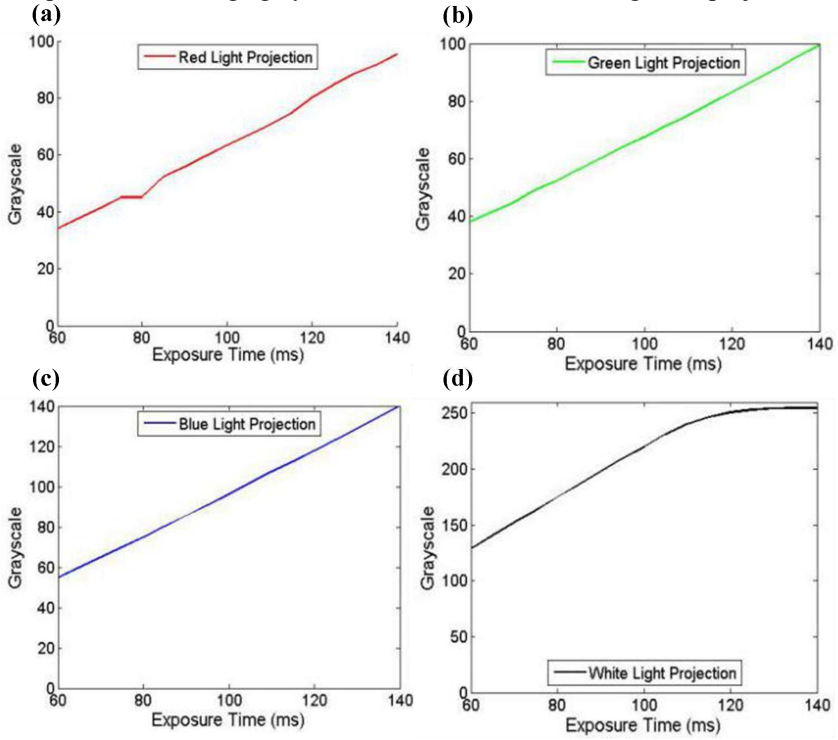

Fig. 5. Characteristic of the camera at different exposure time. (a) Red light projection. (b) Green light projection. (c) Blue light projection. (d) White light projection.

After adjusting the exposure time, the grayscale of the whiteboard is consistent, as shown in Fig. 4(c). For example, we take an object that has four colors on the surface as the measured object, as shown in Fig. 6(a). We can obtain the correct color by synthesizing the captured images according to Eq. (1). The extracted color texture is shown in Fig. 6(b).

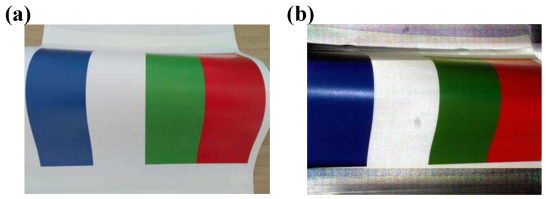

Fig. 6. The color texture extraction. (a) The colorful object. (b) The extracted color texture.

C. Pixel-level color adjustment of the projected image

Since different color on the object surface can absorb different wavelength of the projected light, the contrast and brightness of the captured images are not uniform based on single color light projection, which will reduce the measurement accuracy. 3D shape reconstruction of colorful objects is still a challenge.

For example, we take the object shown in Fig. 7(a) as the measured object. Figures 7(b)~(d) are the captured images by a B/W camera based on blue, green and red light projection. It can be seen that no matter what color light is projected to colorful objects, the intensity of the captured image on the white surface is relatively high. When we project blue light, the brightness of the captured image on the blue surface is relatively high, however, the brightness of the captured image on the other color surfaces is relatively low. In addition, when we project green light, the brightness of the captured image on the green surface is relatively high, and when we project red light, the brightness of the captured image on the red surface is relatively high.

We further discuss the contrast of the captured images. First, we project the white fringe pattern, and the captured image is shown in Fig. 7(e). We extract a row of pixels at the red dotted line in Fig. 7(e) to get its intensity and contrast, as shown in Fig. 7(f). It can be seen that the intensity and contrast of the white surface is higher, but the intensity and contrast of the other color surfaces are lower. We further project the blue, green and red fringe patterns, and then extract three rows of pixels at the red dashed line in Fig. 7(e) to obtain the intensity and contrast, as shown in Fig. 7(g).

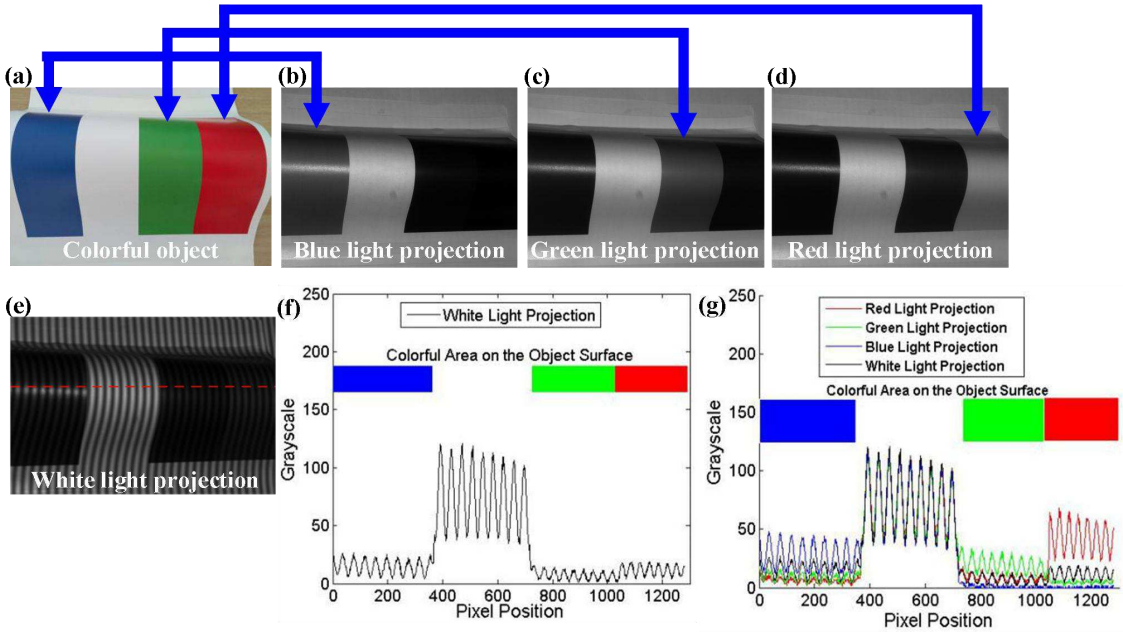

Fig. 7. Pixel-level color. (a) Colorful object. (b) The captured image by a B/W camera based on blue light projection. (c) The captured image by a B/W camera based on green light projection. (d) The captured image by a B/W camera based on red light projection. (e) The captured fringe pattern by a B/W camera based on white light projection. (f) The grayscale of the red dotted line in Fig. 8(e). (f) The grayscale of the red dotted line in Fig. 8(e) based on different light projection.

Obviously, the brightness and contrast of the blue surface when projecting blue light is higher than the brightness and contrast of the blue surface when projecting other colors. The brightness and contrast of the green surface when projecting green light is higher than the brightness and contrast of the green surface when projecting other colors. The brightness and contrast of the red surface when projecting red light is higher than the brightness and contrast of the red

surface when projecting other colors. Subsequently, we project the blue, green and red fringe patterns, respectively. We extract the pixels at the red dashed line in Fig. 7(e), and the intensity and contrast in Fig. 7(g) are obtained. Obviously, the brightness and contrast on the blue surface based on blue light projection are higher than those based on other color light projections. Similarly, the brightness and contrast on the green surface based on green light projection are higher than those based on other color light projections. In addition, the brightness and contrast on the red surface based on red light projection are higher than those based on other color light projections.

Therefore, for 3-D shape measurement of colorful objects, we can obtain the surface color texture of the object according to the method proposed in Section B, and then adjust the color of each pixel in the projected image according to the method proposed in Section A. Pixel-level color adjustment of the projected image can be expressed as

$$C_P(x_P,y_P)=cat(3,I_C^{Red}(x_C,y_C),I_C^{Green}(x_C,y_C),I_C^{Blue}(x_C,y_C)), \tag{7}$$

where $C_P(x_P,y_P)$ represents the color of the pixel (x_P,y_P) on the projected image, $I_C^{Red}(x_C,y_C)$, $I_C^{Green}(x_C,y_C)$ and $I_C^{Blue}(x_C,y_C)$ represent the grayscale of the pixel (x_C,y_C) on the captured image when RGB light is projected.

Through the method described in Section A, the pixel (x_P,y_P) on the projected image corresponding to the pixel (x_C,y_C) on the captured image can be obtained.

D. Estimation of the optimal projection pixel intensity and camera exposure time

The intensity of the captured image is mainly related to the intensity of the projected image, the reflectivity of the object surface, the ambient light and the camera sensitivity, as shown in Fig. 8. Because the aperture of the camera lens needs to be adjusted manually, so we fixed it in this work. Eq. (4) can be rewritten as

$$\begin{aligned} I_C^n(x_C,y_C) &= C_T\left[r(x_C,y_C)I_P^n(x_P,y_P)+A_L(x_C,y_C)\right] \\ &= C_T\{r(x_C,y_C)\{A(x_P,y_P)+B(x_P,y_P) \\ &\quad \cos[\varphi(x_P,y_P)+2\pi(n-1)/N]\}+A_L(x_C,y_C)\} \end{aligned}. \tag{8}$$

To determine the optimal exposure time and pixel intensity of the projected image, r and A_L need to be estimated in advance. Subsequently, we can select the optimal exposure time and pixel intensity of the projected image, i.e. parameters C_T and A (B=A) in Eq. (8).

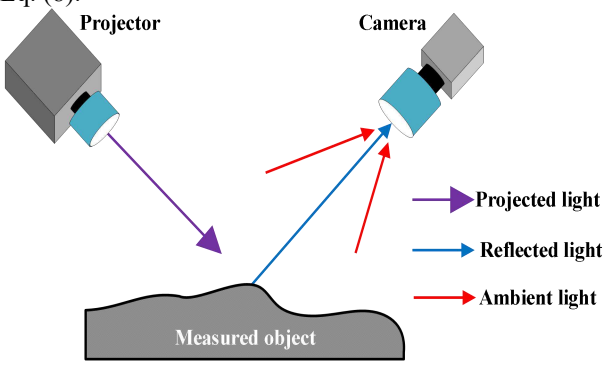

Fig. 8. Factors affecting the intensity of captured image.

In this work, we project two additional images to estimate r and A_L. The grayscale of the first and second projection images is 0 and 100, respectively. We project and capture them, r and A_L can be calculated according to Eq. (9).

$$\begin{cases} A_L^*(x_C,y_C)=\dfrac{I_C^0(x_C,y_C)}{C_T} \\ r^*(x_C,y_C)=\dfrac{I_C^{100}(x_C,y_C)}{100C_T}-\dfrac{A_L(x_C,y_C)}{100} \end{cases}, \tag{9}$$

where I_C^0 and I_C^{100} represents the captured fringe pattern when the intensity of the projected image is 0.

We substitute A_L^* and r^* into Eq. (8), Eq. (8) can be rewritten as

$$I_C^n(x_C,y_C)=C_T\left[r^*(x_C,y_C)I_P^n(x_P,y_P)+A_L^*(x_C,y_C)\right]. \tag{10}$$

The pixel (x_P,y_P) on the projected image corresponding to the pixel (x_C,y_C) on the captured image has been obtained according to Section A. The optimal projection pixel intensity and camera exposure time can be obtained by the following method.

Step 1: For the captured fringe pattern in Eq. (10), the fringe modulation, γ, can be expressed as

$$\gamma(x,y)=\frac{b_C^n(x_C,y_C)}{a_c^n(x_C,y_C)}=\frac{r^*(x_C,y_C)B(x_P,y_P)}{r^*(x_C,y_C)A(x_P,y_P)+A_L^*(x_C,y_C)}, \tag{11}$$

The larger the γ, the higher the fringe signal-to-noise ratio (SNR), so the average and modulation intensity of the projected fringe pattern satisfy the following relationship.

$$B(x_P,y_P)=A(x_P,y_P)+A_L^*(x_C,y_C)/r^*(x_C,y_C). \tag{12}$$

Step 2: We use Genetic algorithm (GA) to optimize I_P^n and C_T in formula (10), and its constraints include: a) The projected image is not saturated, but as close to 255 as possible, and the ratio of the average and modulation intensity of the projected image is as close as possible to formula (12). b) The captured image is not saturated, but as close to 255 as possible.

E. High-precision phase calculation

Three-step phase-shifting (PS) method is adopted to calculate the wrapped phase.

$$\psi_{3\text{-step}}(x,y)=\tan^{-1}\left\{\frac{\sqrt{3}[I_2(x,y)-I_3(x,y)]}{2I_1(x,y)-I_2(x,y)-I_3(x,y)}\right\}, \tag{13}$$

where $\psi_{3\text{-}step}(x, y)$ represents the wrapped phase using three-step PS. Due to the application of the $\tan^{-1}$ operator, $\psi_{3\text{-}step}$ is between $-\pi$ and π when considering the sign of the real and imaginary parts [32–35].

The real phase can be written as

$$\varphi(x,y)=2\pi k+\psi_{3\text{-step}}(x,y), \tag{14}$$

where k is the fringe order, the process of obtaining real phase is called phase unwrapping.

Phase unwrapping algorithms are generally divided into two categories, spacial phase unwrapping (SPU) and temporal phase unwrapping (TPU) algorithms. TPU algorithms need to project and capture fringe sequences with different frequencies, but its phase unwrapping accuracy and computation reliability are very high. At present, three pitches unwrapping algorithm (TPUA), negative exponential unwrapping algorithm (NEUA) and three pitches heterodyne unwrapping algorithm (TPHUA) are widely used. TPHUA only needs three frequency fringe sequences, while ensuring higher reliability in the unwrapping stage [36-38].

Principle of TPHUA is as follows. Three frequencies of the projected fringe patterns are $f1=S+\sqrt{S}+1$ (S is a constant), $f2=S$ and $f3=S-\sqrt{S}$, respectively. $\psi^{S+\sqrt{S}+1}$, ψ^{S} and $\psi^{S-\sqrt{S}}$ are calculated by three-step PS. $\psi^{\sqrt{S}+1}$ is obtained from $\psi^{S+\sqrt{S}+1}$ and ψ^{S}, $\psi^{\sqrt{S}}$ is obtained from ψ^{S} and $\psi^{S-\sqrt{S}}$. At last, ψ^1 is calculated from $\psi^{\sqrt{S}+1}$ and $\psi^{\sqrt{S}}$. $\varphi^1=\psi^1$, the unwrapped phase with higher frequency can be obtained using the Formula (15).

$$\begin{cases}\varphi^{f_i}(x,y)=\psi^{f_i}(x,y)+R^{f_i}(x,y)\times 2\pi\\ R^{f_i}(x,y)=INT\left[\dfrac{(f_i/f_{(i-1)})\times\varphi^{f_{(i-1)}}(x,y)-\psi^{f_i}(x,y)}{2\pi}\right]\end{cases}, \tag{15}$$

where ψ^f and φ^f represents the wrapped and unwapped phase with the frequency f, *INT* is a *round* operator.

III. EXPERIMENTS

The structure of the 3-D measurement system is shown in Fig. 9, including a projector, a camera and a personal computer. The computer reconstructs 3-D shape after processing the captured fringe patterns.

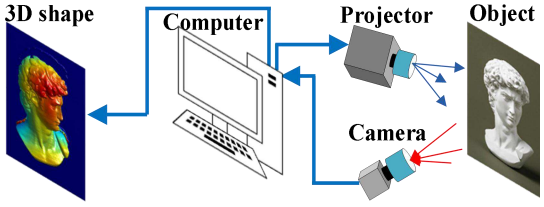

Fig. 9. Structure of the 3-D measurement system.

A. Experimental results of the smooth metal objects

After metal is processed at high speed on various machines, its surface is often very smooth, so the captured image has non-diffuse reflection characteristics. Figure 10(a) is a captured image of a workpiece processed at a high speed on a CNC milling machine. The original projection fringe pattern is shown in Fig. 10(b). Based on the adaptive projection fringe optimization method proposed in this paper, we can get a projection fringe patter shown in Fig. 10(c). It can be seen from Fig. 10(c) that for the different reflectivity of the measured surface, the pixel intensity on the corresponding

projection image is adjusted adaptively. Since there are no colors on the surface, the adaptive projection fringe pattern is pure color. For colored surfaces, we will analyze and compare in Section 3.2. Figure 10(d) is an original captured fringe pattern. The high reflectance area of the metal surface is overexposed, and the low reflectance area is too dark. Over-exposure will cause phase calculation errors, while over-darkness will reduce image contrast. Figure 10(e) is a captured fringe pattern based on the adaptive fringe projection proposed in this paper. The overexposed area is significantly improved, and the pixels in the over dark area become brighter. In fact, the intensity and contrast of the over dark area are improved. We compare the 3-D reconstruction surfaces, and the results are shown in Figs. 10(f) ~ (g). Using original fringe patterns, there are holes or wrinkles in the 3-D surface shape of the overexposed and over-dark areas. However, the 3-D surface shape using the optimized captured fringe patterns has been significantly improved.

In addition, regarding the measurement efficiency, the proposed method needs to add two images when calculating the adaptive projection fringe pattern. When extracting the color texture of the surface of the measured object, three images are added. Therefore, the proposed method only needs to add 5 images. However, references [6]-[8] require a large number of camera exposure time adjustment or projection image intensity adjustment, and the number of additional images is very large. We compare the proposed method with references [6] and [7], the number of additional projection fringes is shown in Table 1, where *N* represents the number of fringe patterns in a set of fringe sequences.

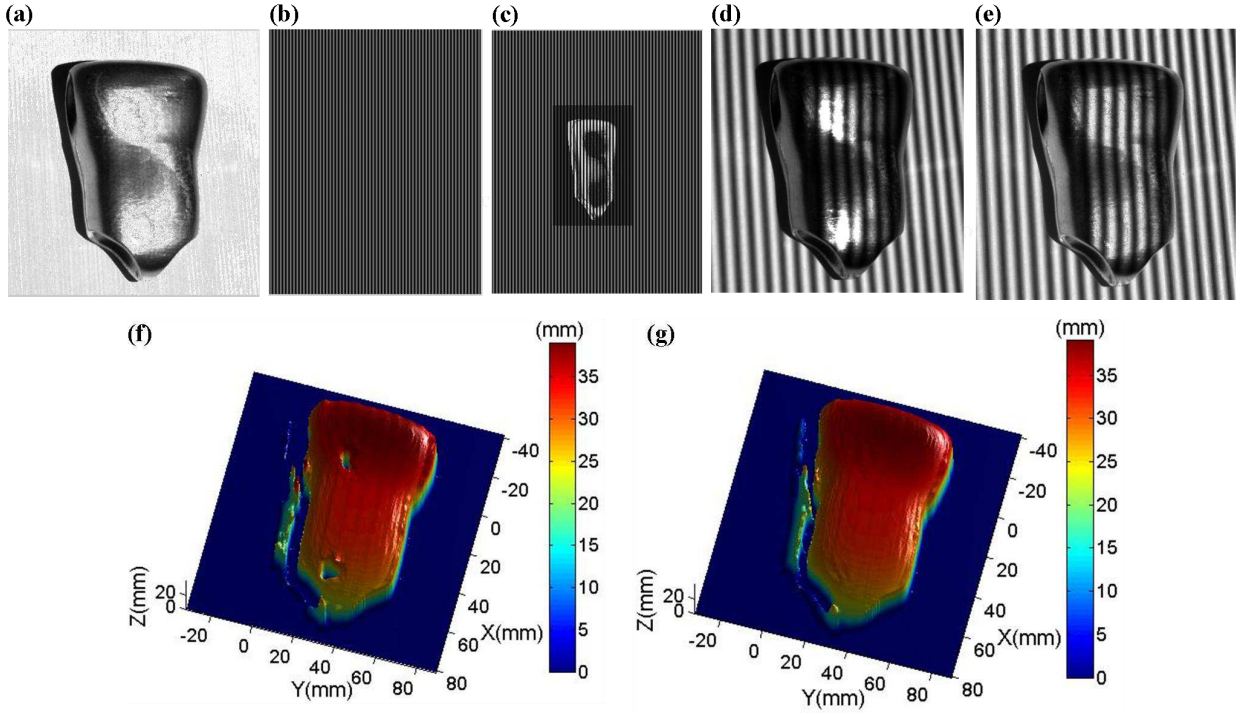

Fig. 10. 3-D shape reconstruction of a metal product 2. (a) A metal product. (b) Original projection fringe pattern. (c) Optimized projection fringe pattern. (d) Original captured fringe pattern. (e) Optimized captured fringe pattern. (f) Reconstructed 3-D surface shape using the original captured fringe patterns. (g) Reconstructed 3-D surface shape using the optimized captured fringe patterns.

Reference [6] uses 23 camera exposure times to get the fringe sequence, and 22 additional sets of fringe sequences are added. Reference [7] obtains fringe sequences with different intensities by using colored light projection, intensity adjustment of the entire projected image, and camera exposure time adjustment. Compared with a set of fringe sequences, 6 sets of fringe sequences are added. However, the method proposed in this paper only needs to add 5 additional fringe patterns to get a good set of fringe patterns. It is worth noting that there is a big difference between the method in this paper and the method in reference [7]. That is, in reference [7], the overall grayscale of the projected fringe pattern is adjusted. The method proposed in this paper is to adjust each pixel on the projected fringe pattern according to the reflectivity of the measured surface.

Table 1. Number of additional fringe patterns.

Method	Ref. [6]	Ref. [7]	The proposed method
Number of additional fringe patterns	22**N*	6**N*	5

To further verify the effectiveness of the proposed method, we take another metal product as the measured objects, as shown in Fig. 11(a). Figure 11(b) is an original projection fringe pattern. Figure 11(c) is an adaptive projection

fringe pattern, and its pixel intensity is adjusted adaptively according to the reflectivity of the measured object. Figure 11(d) is an original captured fringe pattern. Figure 11(e) is an optimized captured fringe pattern based on the adaptive fringe projection proposed in this paper. Figures 11(f) ~ (g) show the 3-D reconstruction surfaces. It can be seen that the 3-D surface shape using the proposed method is greatly improved.

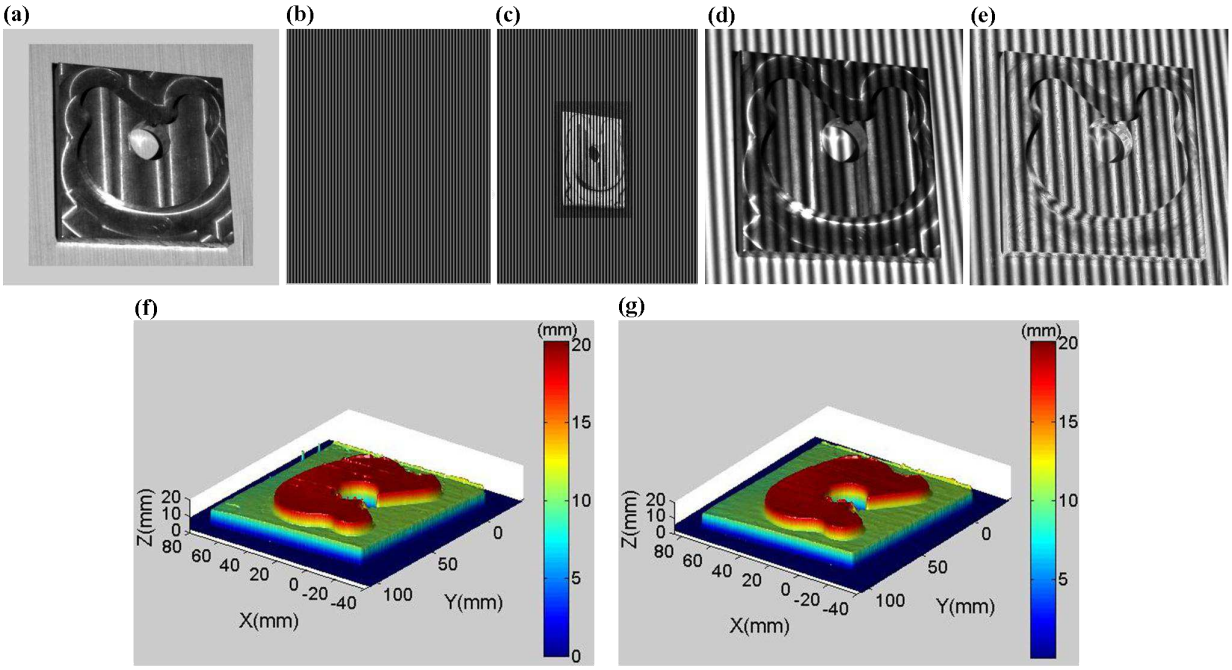

Fig. 11. 3-D shape reconstruction of another metal product 2. (a) Another metal product. (b) Original projection fringe pattern. (c) Optimized projection fringe pattern. (d) Original captured fringe pattern. (e) Optimized captured fringe pattern. (f) Reconstructed 3-D surface shape using the original captured fringe patterns. (g) Reconstructed 3-D surface shape using the optimized captured fringe patterns.

To achieve the quantitative comparisons, we utilize RMSE (root mean square error) to evaluate the 3-D shape precision, as shown in Table 2. It can be seen that the measurement error of the proposed method is reduced by 59.9%.

Table 2. Quantitative comparison (RMSE)

Method	Without the proposed method	With the proposed method
RMSE	0.0681	0.0273

B. Experimental results of colorful objects

Figure 12(a) shows an object with different colors on the surface. When the fringe pattern is not projected, the ambient light can be considered as white light, and the image captured by the camera is shown in Fig. 12(b). It can be seen that different colors have different absorption and reflectance of white light, and the white surface has the highest reflectance. Figure 12(c) is the original projection fringe pattern. Figure 12(d) is the optimized projection fringe pattern obtained by the method proposed in this paper. The pixel grayscale and color are adjusted according to the reflectivity and color of the object surface. Figures 12(e) ~ (g) are the captured images during red light projection, green light projection and blue light projection. Figure 12(h) is the image captured based on the method proposed in this paper. It can be seen that Figure 12(h) is clearer than Figures 12(e) ~ (g), especially the contrast and brightness of the non-white areas are better. Figures 12(i) ~ (k) shows the 3-D reconstructed shapes during red light projection, green light projection and blue light projection. 3-D reconstruction surface corresponding to the blue and green areas during red light projection has a large number of cavities or wrinkles. 3-D reconstruction surface corresponding to the blue and red areas during green light projection also has a large number of cavities or wrinkles. 3-D reconstruction surface corresponding to the green and red areas during blue light projection has a lot of cavities or wrinkles as well. Figure 12(l) is a 3-D reconstruction shape based on the method proposed in this paper. Its contour is complete and the contour wrinkles are significantly reduced.

In order to further verify the effectiveness of the proposed method, we use another colored object as the measured object. Through the comparison in Fig. 13, it is further verified the effectiveness of the proposed method.

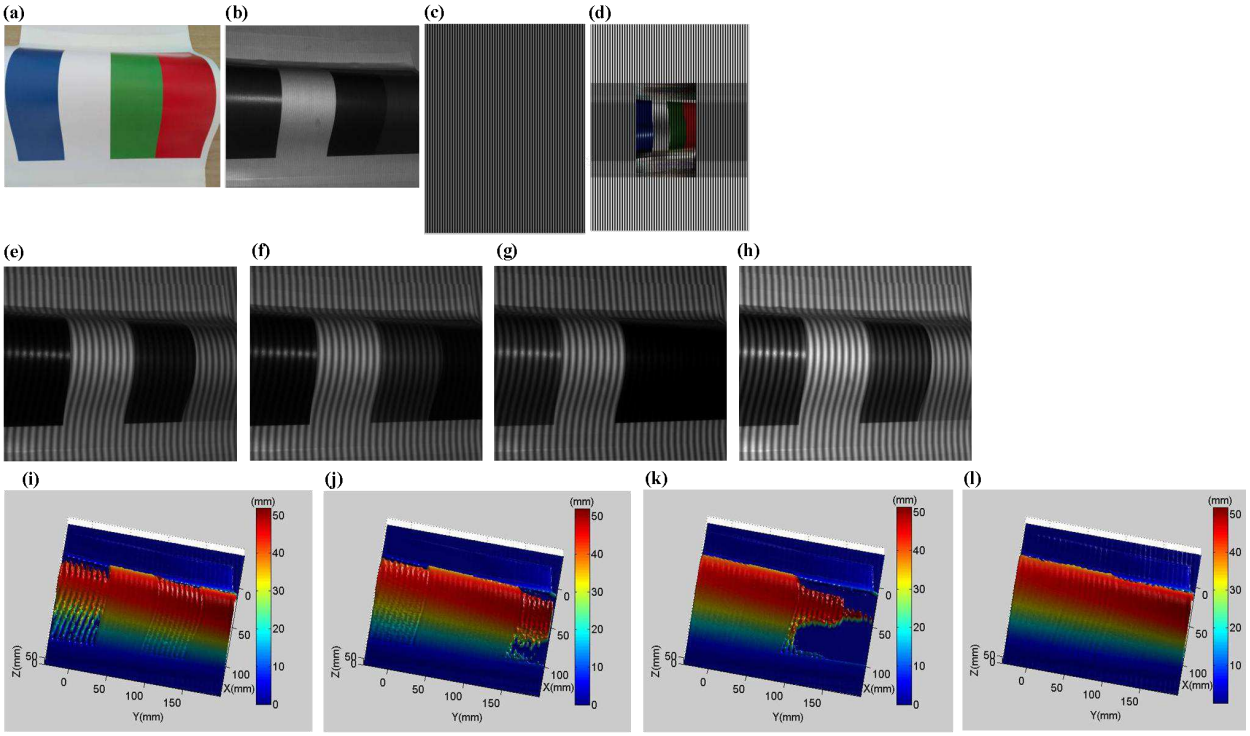

Fig. 12. 3-D shape reconstruction of a colorful object. (a) A colorful object. (b) A captured image without fringe projection. (c) Original projection fringe pattern. (d) Optimized projection fringe pattern. (e) A captured fringe pattern during red light projection. (f) A captured fringe pattern during green light projection. (g) A captured fringe pattern during blue light projection. (h) Optimized captured fringe pattern using the method proposed in this paper. (i) Reconstructed 3-D surface shape during red light projection. (j) Reconstructed 3-D surface shape during green light projection. (k) Reconstructed 3-D surface shape during blue light projection. (l) Reconstructed 3-D surface shape using the method proposed in this paper.

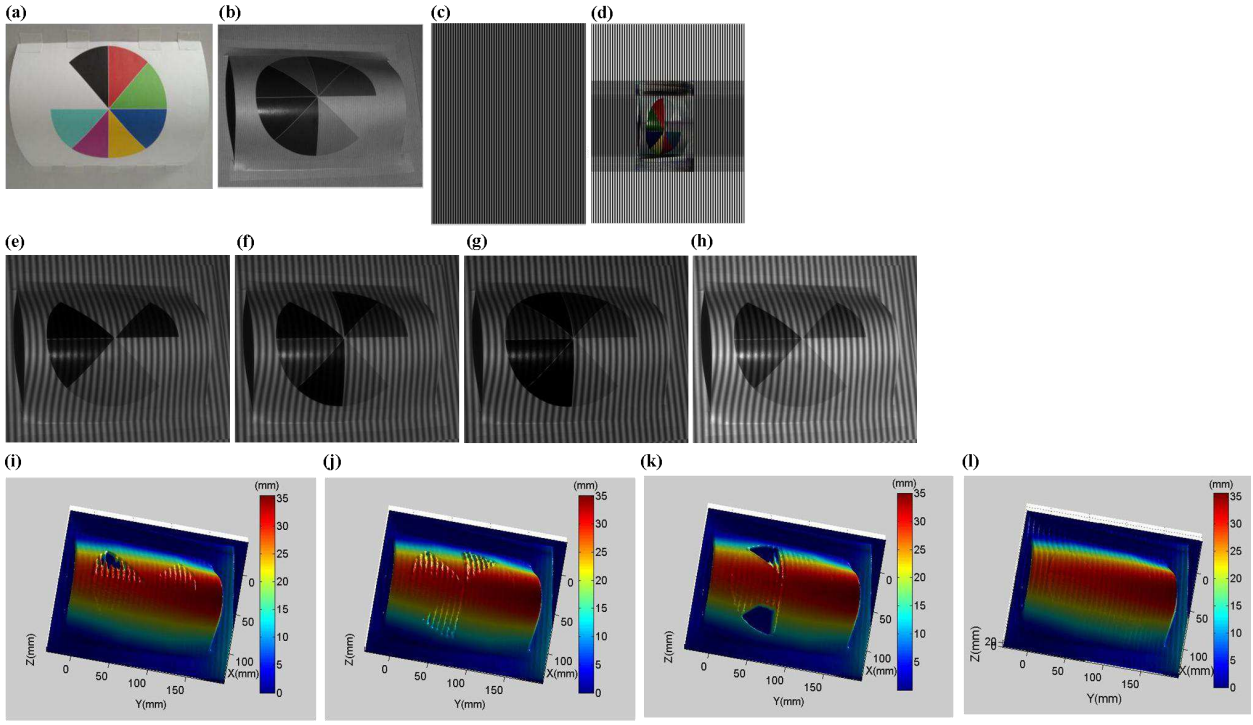

Fig. 13. 3-D shape reconstruction of a colorful object. (a) Another colorful object. (b) A captured image without fringe projection. (c) Original projection fringe pattern. (d) Optimized projection fringe pattern. (e) A captured fringe pattern during red light projection. (f) A captured fringe pattern during green light projection. (g) A captured fringe pattern during blue light projection. (h) Optimized captured fringe pattern using the method proposed in this paper. (i) Reconstructed 3-D surface shape during red light projection. (j) Reconstructed 3-D surface shape during green light projection. (k) Reconstructed 3-D surface shape during blue light projection. (l) Reconstructed 3-D surface shape using the method proposed in this paper.

IV. DISCUSSION

The advantages of the proposed method include the following aspects.

(1) The proposed method can adaptively adjust the pixel color and intensity of the projected image, exposure time of the camera according to the color information and reflectivity of the measured object surface, which improves the captured image quality as much as possible. Therefore, the method has good 3-D measurement accuracy.

(2) The proposed method only needs 5 additional images. Compared with the existing method, the proposed method requires fewer additional images, thus improving the measurement efficiency.

(3) Compared with the existing methods, the proposed method can effectively reconstruct the 3-D surface shape of reflective objects as well as the 3-D surface shape of colored objects, so the scope of application is wider.

Although this method need a pre-matching operation, there is no need to operate in the future once the measurement system is fixed.

V. CONCLUSION

This paper proposed a high-precision and high-efficiency 3-D surface reconstruction method suitable for colored objects and reflective objects. First of all, we propose a rough matching method based on Gray coding and a fine matching method based on image pixel displacement, thus establishing the pixel correspondence between the projected image and the captured image. Second, we use a B/W camera to extract the surface color texture through three additional images. Third, we estimate the color of the measured surface through RGB color light projection. Fourth, we estimate the reflectivity and ambient light interference through the other two additional images, and find the best projection pixel intensity and camera exposure time based on GA. The proposed method not only has good 3-D surface reconstruction accuracy, but also has a small number of additional images, and can be widely used in the 3-D measurement of various colored and reflective objects.

REFERENCES

[1] S. Zhang, “High-speed 3D shape measurement with structured light methods: A review,” Opt. Lasers Eng., vol. 106, pp. 119–131, Jul. 2018.
[2] C. Zuo, Q. Chen, G. H. Gu, S. J. Feng, F. X. Y. Feng, “High-speed three-dimensional profilometry for multiple objects with complex shapes,” Opt. Express, vol. 20, no. 17, pp. 19493–19510, Aug. 2012.
[3] J. H. Wang, Y. G. Zhou, Y. X. Yang, “Rapid 3D measurement technique for colorful objects employing RGB color light projection,” Appl. Opt., vol. 59, no. 9, pp. 1907–1915, Mar. 2020.
[4] H. Nguyen, D. Nguyen, Z. Wang, H. Kieu, M. Le, “Real-time, high-accuracy 3D imaging and shape measurement,” Appl. Opt., vol. 54, no. 1, pp. 9-17, Jan. 2015.
[5] Z. J. Wu, W. B. Guo, Q. C. Zhang, “High-speed three-dimensional shape measurement based on shifting Gray-code light,” Opt. Express, vol. 27, no. 16, pp. 22631–22644, Aug. 2019.
[6] S. Zhang and S.-T. Yau, “High dynamic range scanning technique,” Opt. Eng., vol. 48, no. 3, doc. 033604, Mar. 2009.
[7] L. Ekstrand and S. Zhang, “Autoexposure for three-dimensional shape measurement using a digital-light-processing projector,” Opt. Eng., vol. 50, no. 12, doc. 123603, Dec. 2011.
[8] G. H. Liu, X. Y. Liu, Q. Y. Feng, “3D shape measurement of objects with high dynamic range of surface reflectivity,” Appl. Opt., vol. 50, no. 23, pp. 4557-4565, Aug. 2011.
[9] H. Z. Jiang, H. J. Zhao, and X. D. Li, “High dynamic range fringe acquisition: A novel 3D scanning technique for high-reflective surfaces,” Opt. Lasers Eng., vol. 50, no. 10, pp. 1484–1493, Oct. 2012.
[10] K. Zhong, Z. W. Li, X. H. Zhou, Y. F. Li, Y. S. Shi, C. J. Wang, “Enhanced phase measurement profilometry for industrial 3D inspection automation. Int. J. Adv. Manuf. Tech., vol. 76, no. 9-12, pp. 1563-1574, Sep. 2014.
[11] J. H. Wang, Y. G. Zhou, Y. X. Yang, “A novel and fast three-dimensional measurement technology for the objects surface with non-uniform reflection,” Results Phys., vol. 57, no. 30, pp. 9172-9182, Mar. 2020.
[12] S. K. Nayar, X. S. Fang, T. Boult, “Separation of Reflection Components Using Color and Polarization,” Int. J. Comput. Vision, vol. 21, no. 3, pp. 163-186, Jan. 1997.
[13] B. Salahieh, Z. Y. Chen, J. J. Rodriguez, R. G. Liang, “Multi-polarization fringe projection imaging for high dynamic range objects,” Opt. Express, vol. 22, no. 8, pp. 10064-10071, Apr. 2014.
[14] S. A. Shafer, “Using Color to Separate Reflection Components,” Color Res. Appl., vol. 10, no. 4, pp. 210-218, Jan. 1984.
[15] R. T. Tan, K. Nishino, K. Ikeuchi, “Separating Reflection Components Based on Chromaticity and Noise Analysis,” IEEE T. Pattern Anal., vol. 26, no. 10, pp. 1373-1379, Oct. 2004.
[16] H. L. Shen, H. G. Zhang, S. J. Shao, J. H. Xin, “Chromaticity-based separation of Reflection components in a single image,” Pattern Recogn., vol. 41, no. 8, pp. 2461-2469, Mar. 2008.
[17] J. W. Park, K. H. Lee, “Inpainting Highlights Using Color Line Projection,” IEICE T. Inf. Syst., vol. 90-d, no. 1, pp. 250-257, Jan. 2007.
[18] R. Benveniste, C. Unsalan, “A Color Invariant for Line Stripe-Based Range Scanners,” Comput. J., vol. 54, no. 5, pp. 738-753, May. 2011.
[19] R. Benveniste, C. Unsalan, “Nary coded structured light-based range scanners using color invariants,” J. Real-Time Image Pr., vol 9, no. 2, pp. 359-377, Nov. 2014.
[20] C. Waddington, J. Kofman, “Analysis of measurement sensitivity to illuminance and fringe-pattern gray levels for fringe-pattern projection adaptive to ambient lighting,” Opt. Laser Technol., vol. 48, no. 2, pp. 251-256, Feb. 2010.

[21] C. Waddington, J. Kofman, “Modified sinusoidal fringe-pattern projection for variable illuminance in phase-shifting three-dimensional surface-shape metrology,” Opt. Eng., vol. 53, no. 8, doc. 084109, Aug. 2014.
[22] C. Waddington, J. Kofman, “Camera-independent saturation avoidance in measuring high-reflectivity-variation surfaces using pixel-wise composed images from projected patterns of different maximum gray level,” Opt. Commun., vol. 333, no. 0, pp. 32-37, Dec. 2014.
[23] D. Li, J. Kofman, “Adaptive fringe-pattern projection for image saturation avoidance in 3D surface-shape measurement,” Opt. Express, vol. 22, no. 8, pp. 9887-9901, Apr. 2014.
[24] G. Babaie, M. Abolbashari, F. Farahi, “Dynamics range enhancement in digital fringe projection technique,” Precis. Eng., vol. 39, pp. 243-251, Jan. 2015.
[25] C. Zhang, J. Xu, N. Xi, J. G. Zhao, Q. Shi, “A Robust Surface Coding Method for Optically Challenging Objects Using Structured Light,” IEEE T. Autom. Sci. Eng., vol. 11, no. 3, pp. 775-788, Jan. 2014.
[26] J. H. Wang, Y. G. Zhou, Y. X. Yang, “Three-dimensional measurement method for nonuniform reflective objects,” IEEE T. Instrum. Meas., vol. 69, no. 11, PP. 9132-9143, Nov. 2020.
[27] G. Sansoni, M. Carocci, and R. Rodella, “Three-dimensional vision based on a combination of gray-code and phase-shift light projection: analysis and compensation of the systematic errors,” Appl. Opt., vol. 38, no. 31, pp. 6565–6573, Nov. 1999.
[28] W. Lohry, V. Chen, S. Zhang, "Absolute three-dimensional shape measurement using coded fringe patterns without phase unwrapping or projector calibration," OPT. Express, vol. 22, no. 2, pp. 1287-1301, Jan. 2014.
[29] D. L. Zheng, F. P. Da, Q. Kemao, H. S. Seah, “Phase-shifting profilometry combined with Gray-code patterns projection: unwrapping error removal by an adaptive median filter,” Opt. Express, vol. 25, no. 5, pp. 4700-4713, Mar. 2017.
[30] Q. Zhang, X. Su, L. Xiang, and X. Sun, “3-D shape measurement based on complementary Gray-code light,” Opt. Lasers Eng., vol. 50, no. 4, pp. 574–579, Apr. 2012.
[31] S. Yu, J. Zhang, X. Yu, X. Sun, and H. Wu, “Unequal-period combination approach of gray code and phaseshifting for 3-D visual measurement,” Opt. Commun., vol. 374, no. 1, pp. 97–106, Apr. 2016.
[32] M. H. Duan, Y. Jin, C. M. XU, X. B. Xu, C. A. Zhu, E. H. Chen, “Phase-shifting profilometry for the robust 3-D shape measurement of moving objects,” Opt. Express, vol. 27, no. 16, pp. 22100-22115, Aug. 2019.
[33] T. Y. Tao, Q. Chen, J. Da, S. J. Feng, Y. Hu, C. Zuo, “Real-time 3D shape measurement with composite phase-shifting fringes and multi-view system,” Opt. Express, vol. 24, no. 18, pp. 20253-20269, Sep. 2016.
[34] F. X. Lu, S. Xing, H. W. Guo, “Self-correction of projector nonlinearity in phase-shifting fringe projection profilometry,” Appl. Opt., vol. 56, no. 25, pp. 7204-7216, Sep. 2017.
[35] J. H. Wang, Y. G. Zhou, Y. X. Yang, “Three-dimensional shape detection for non uniform reflective objects: Combination of color light projection and camera’s exposure adjustment,” IEEE Sens. J., vol. 20, no. 19, pp. 11474-11483, Sep. 2020.
[36] C. Zuo, L. Huang, M. L. Zhang, Q. Chen, and A. Asundi, “Temporal phase unwrapping algorithms for fringe projection profilometry: A comparative review,” Opt. Lasers Eng., vol. 85, pp. 84-103, Oct. 2016.
[37] S. Xing, and H. Guo, “Temporal phase unwrapping algorithms for fringe projection profilometry aided by recursion of Chebyshev polynomials,” Appl. Opt., vol. 56, no. 6, pp. 1591-1602, Feb. 2017.
[38] Y. Xing, C. Quan, C. J. Tay, “A generalized multi-sensitivity temporal phase unwrapping method for absolute phase retrieval,” Opt. Laser Technol., vol. 96, pp. 290-298, Nov. 2017.

Acknowledgements

This work was funded by the Shaanxi Key Laboratory of Complex System Control and Intelligent Information Processing (Contract No. 2020CP07), Xi’an University of Technology.

Author Contributions

Jianhua Wang designed the research, collected, analyzed and interpreted the data, and drafed the manuscript. Yanxi Yang reviewed the manuscript for important intellectual content. Yuguo Zhou analysed and interpreted the data.

Additional Information

Competing Interests: The authors declare no competing interests.

Figures

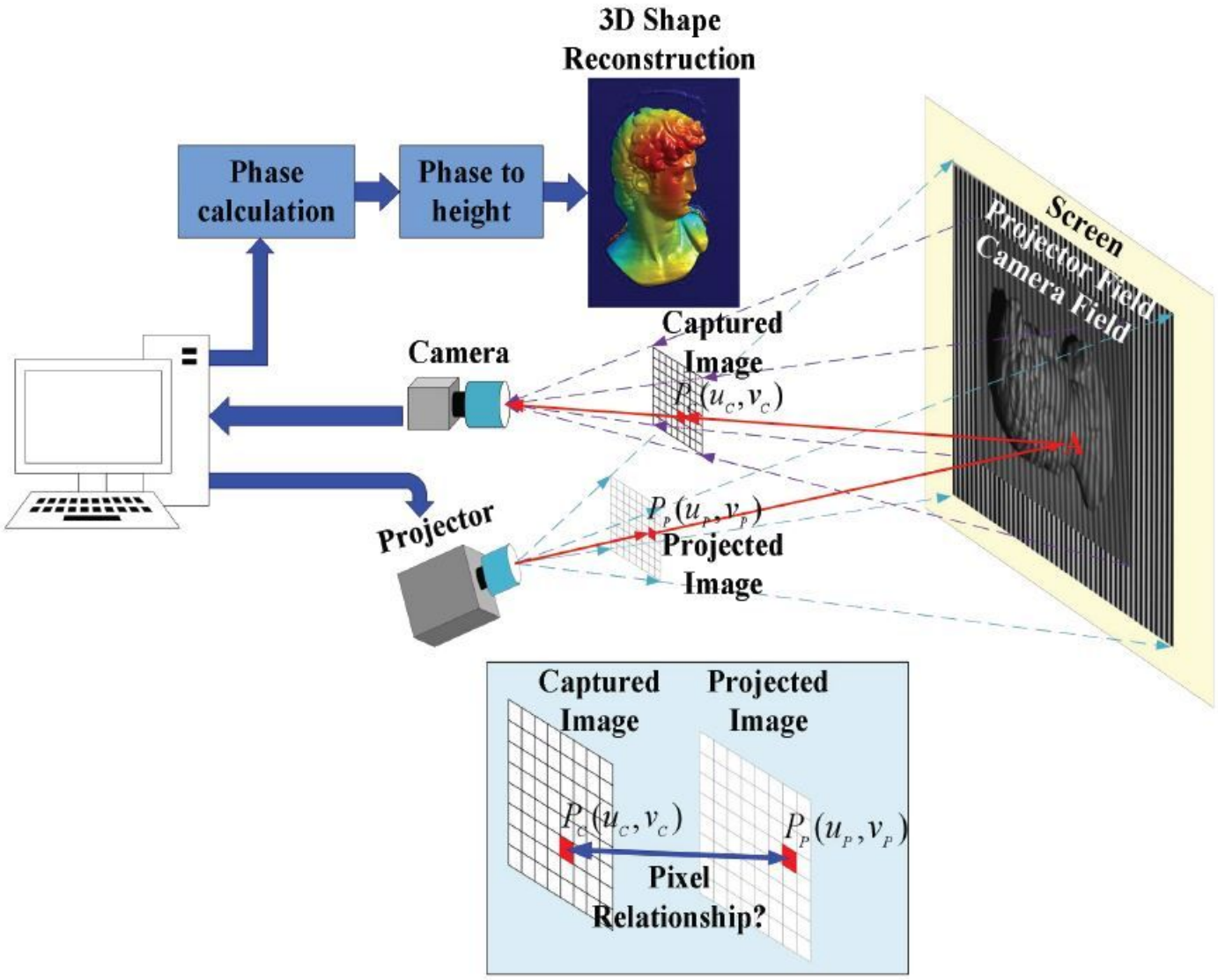

Figure 1

Camera and projector field of view.

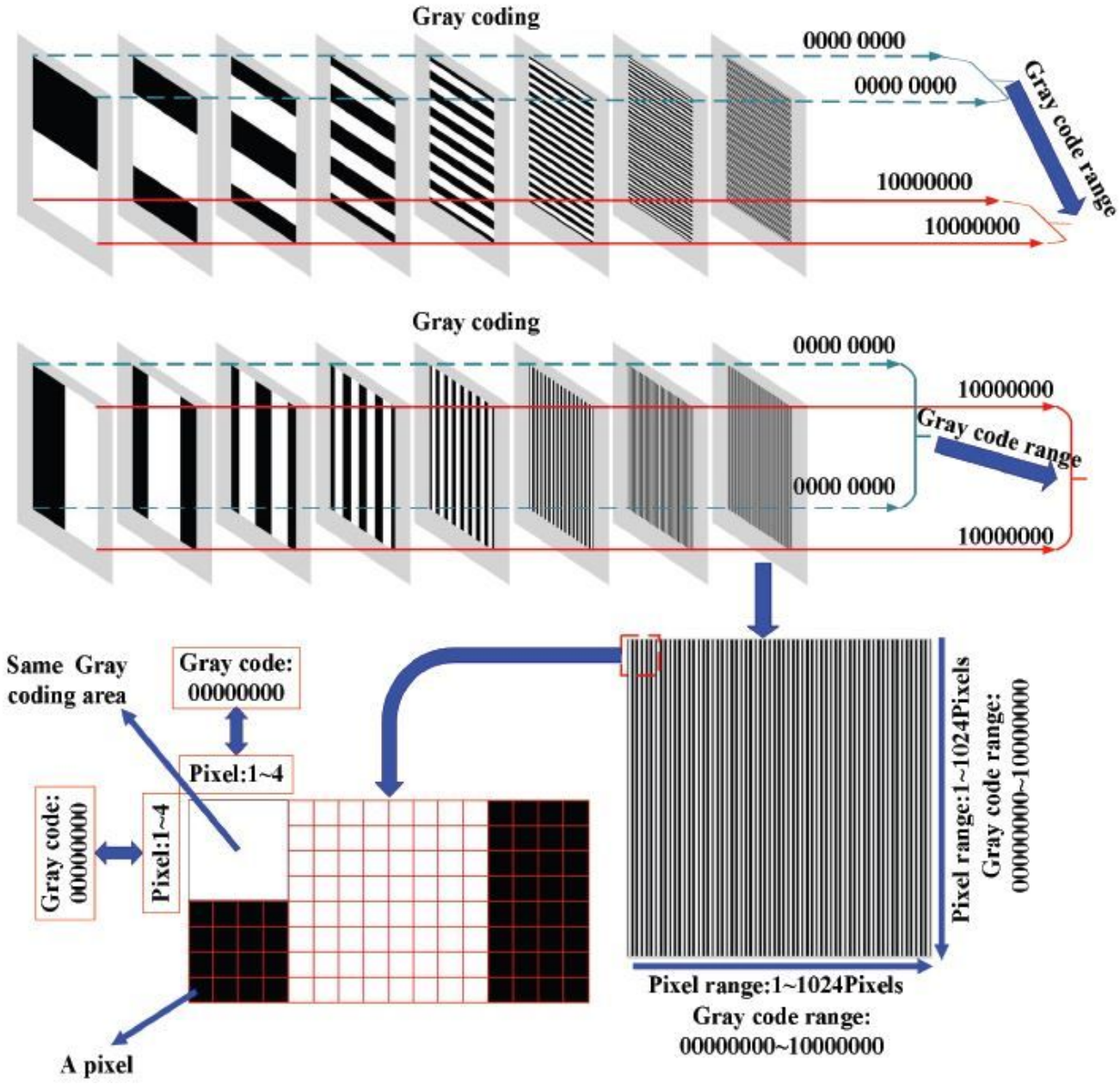

Figure 2

Rough coding of the entire projection pattern based on Gray coding.

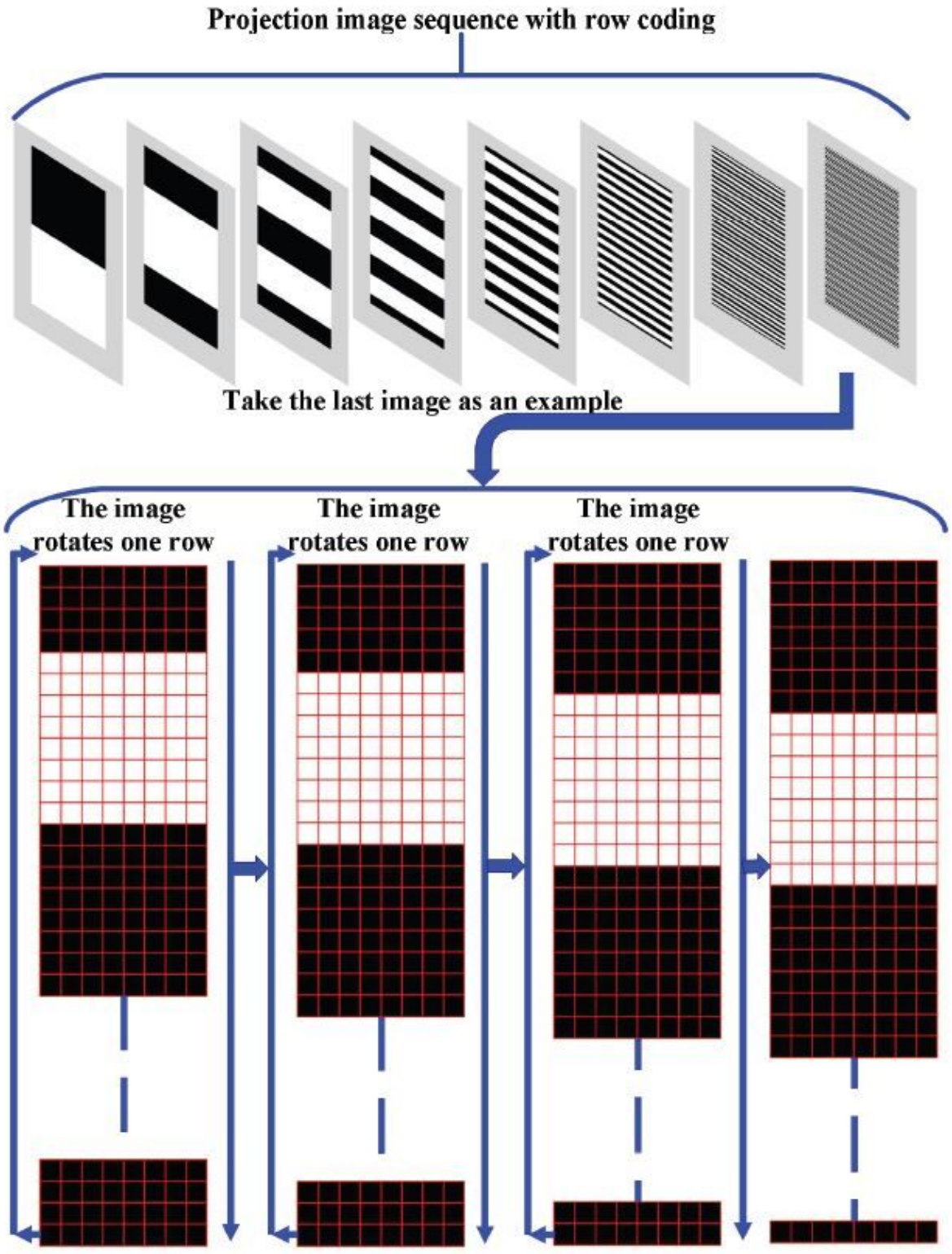

Figure 3

Fine coding of row.

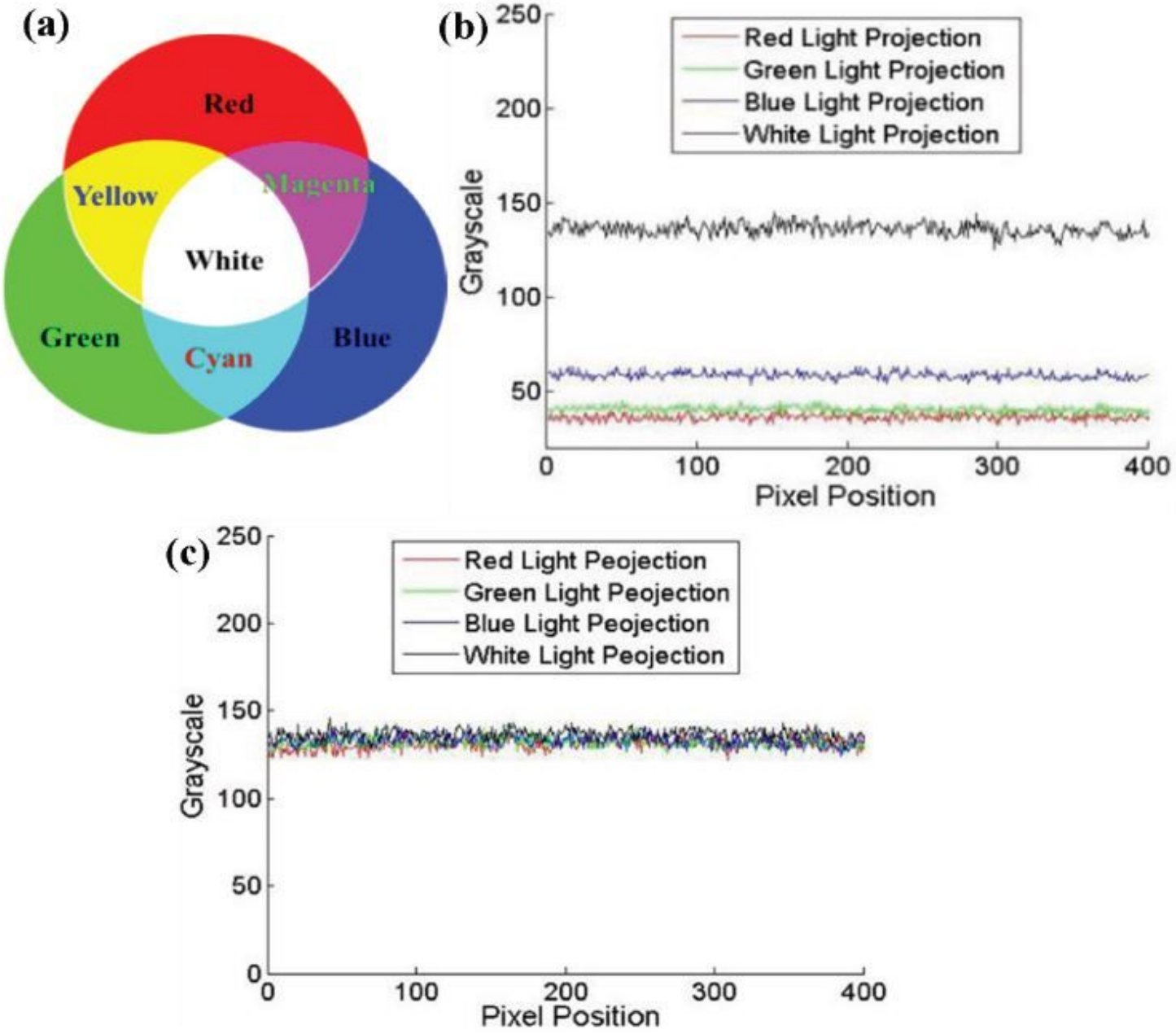

Figure 4

The principle of color texture extraction using B/W camera. (a) Additive method of three primary colors. (b) The intensity of the captured images employing white, red, green and blue light projection. (c) The intensity of the captured images after the exposure time adjustment.

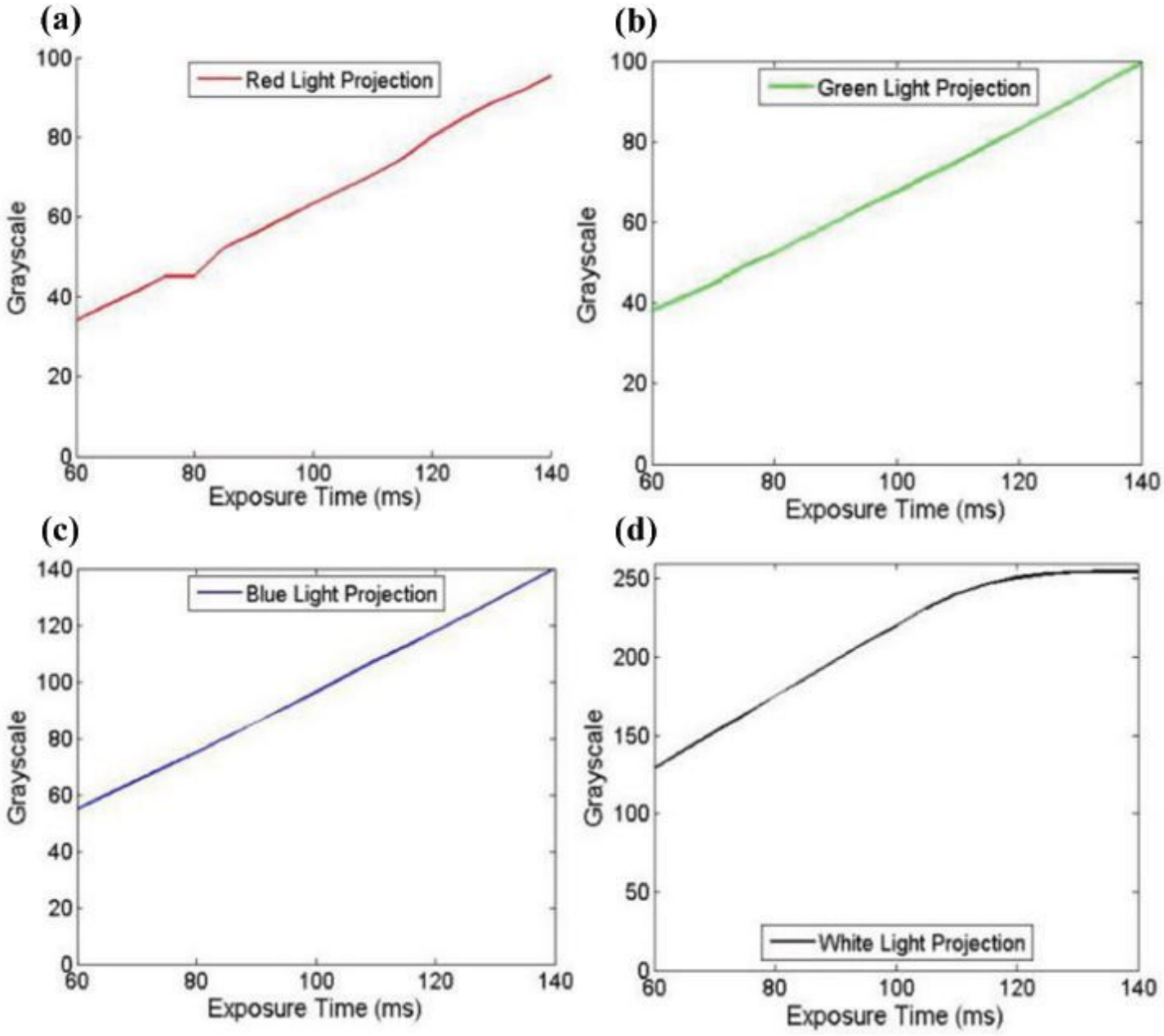

Figure 5

Characteristic of the camera at different exposure time. (a) Red light projection. (b) Green light projection. (c) Blue light projection. (d) White light projection.

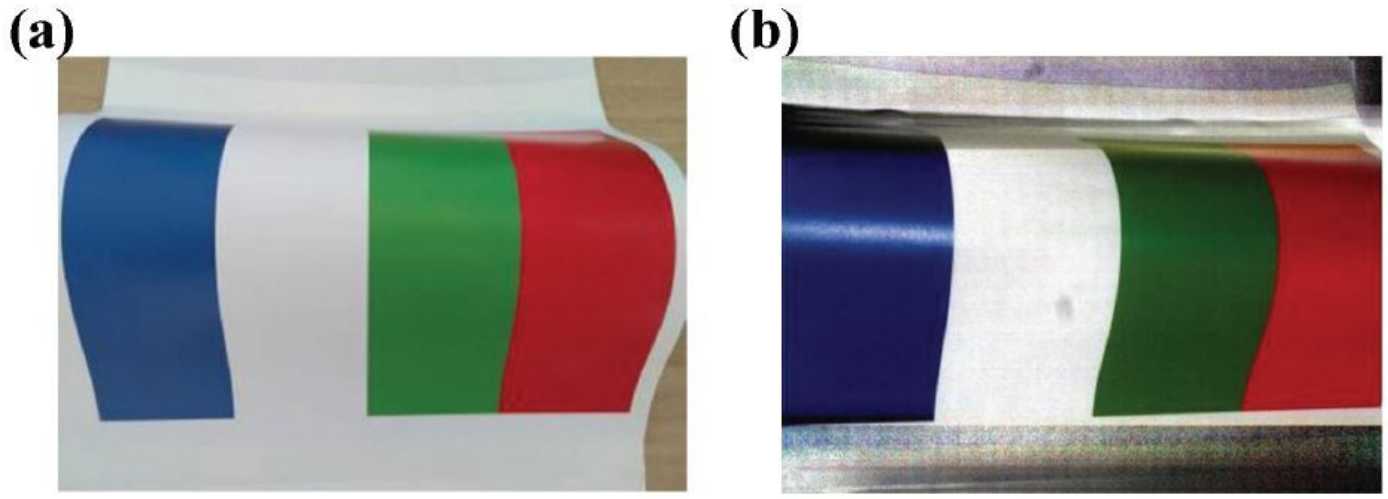

Figure 6

The color texture extraction. (a) The colorful object. (b) The extracted color texture.

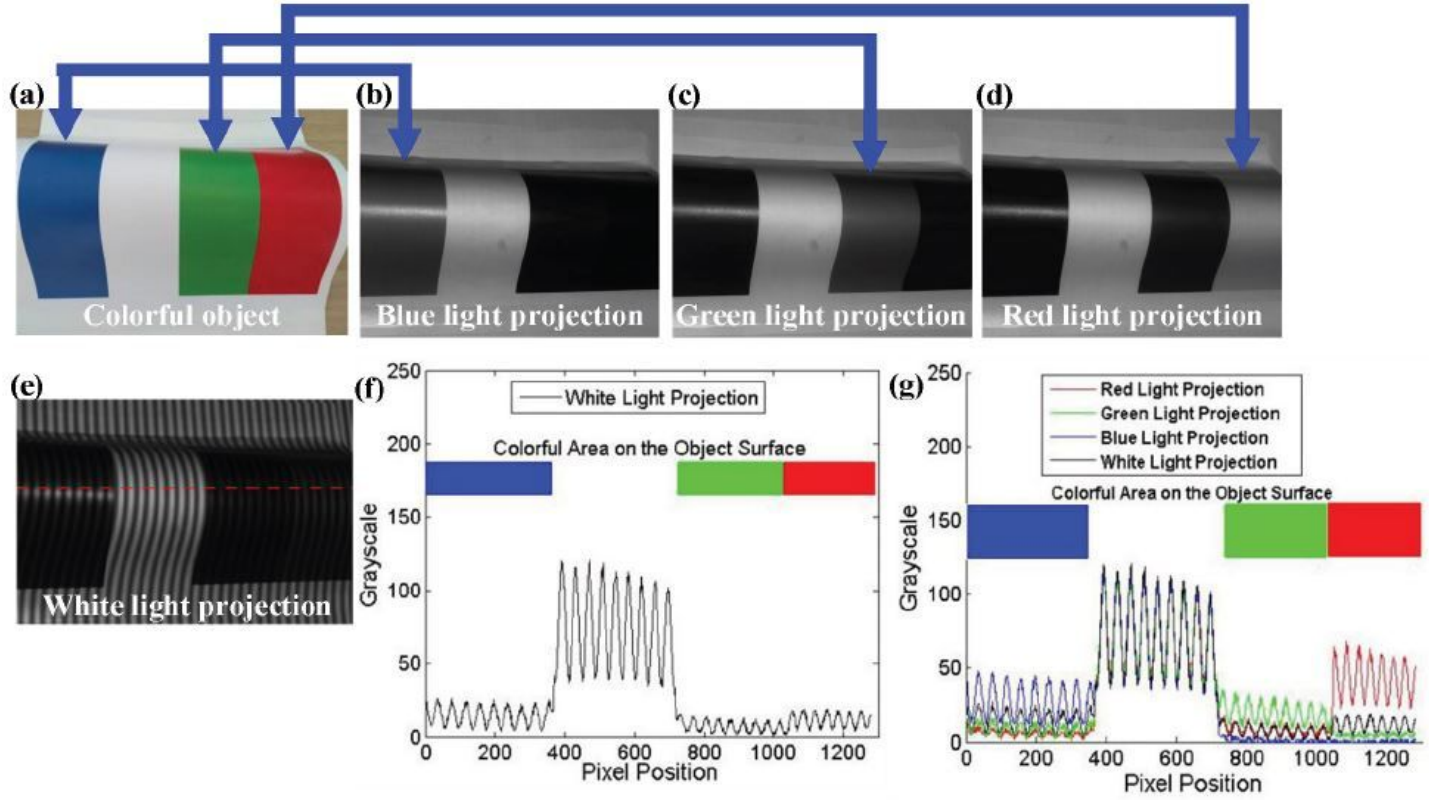

Figure 7

Pixel-level color. (a) Colorful object. (b) The captured image by a B/W camera based on blue light projection. (c) The captured image by a B/W camera based on green light projection. (d) The captured image by a B/W camera based on red light projection. (e) The captured fringe pattern by a B/W camera based on white light projection. (f) The grayscale of the red dotted line in Fig. 8(e). (f) The grayscale of the red dotted line in Fig. 8(e) based on different light projection.

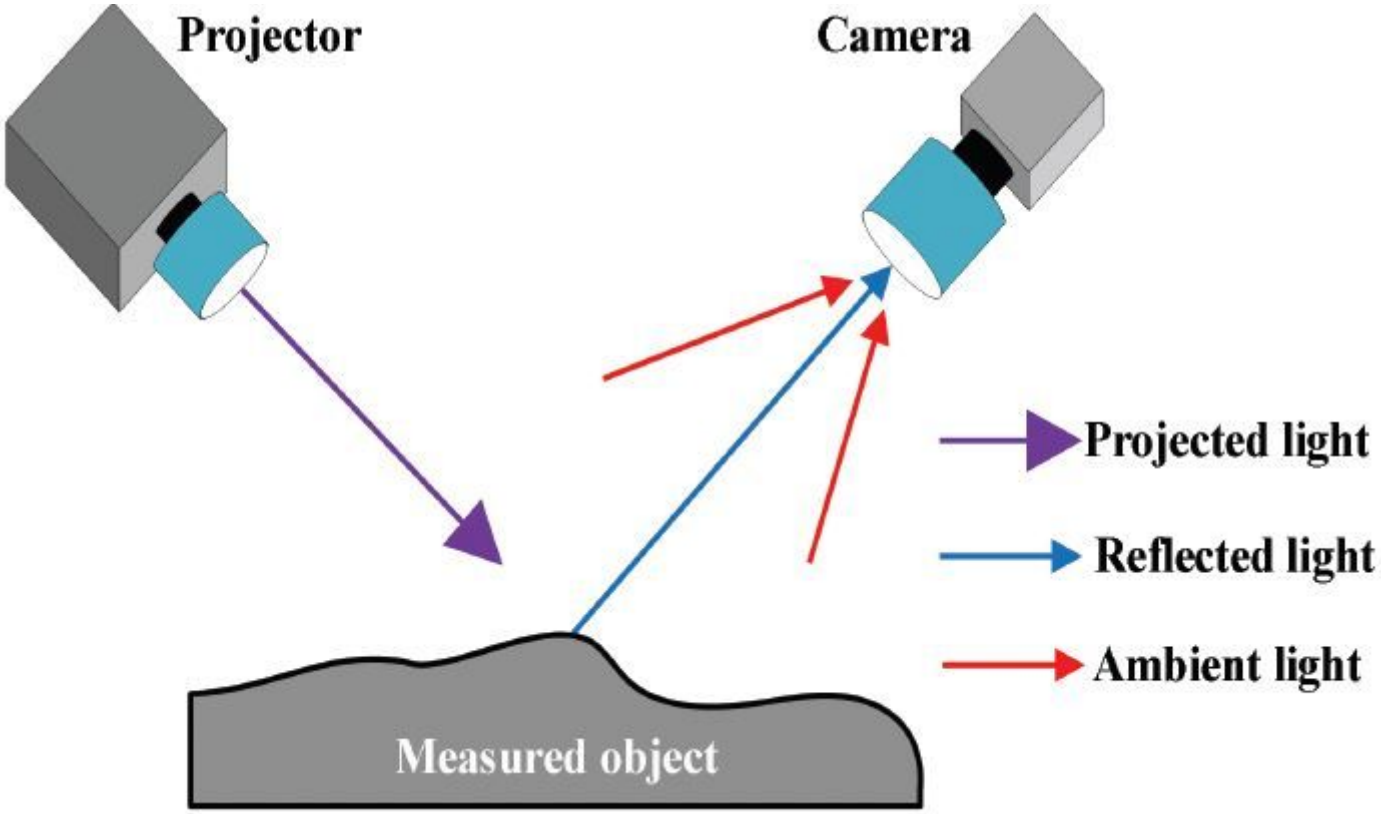

Figure 8

Factors affecting the intensity of captured image.

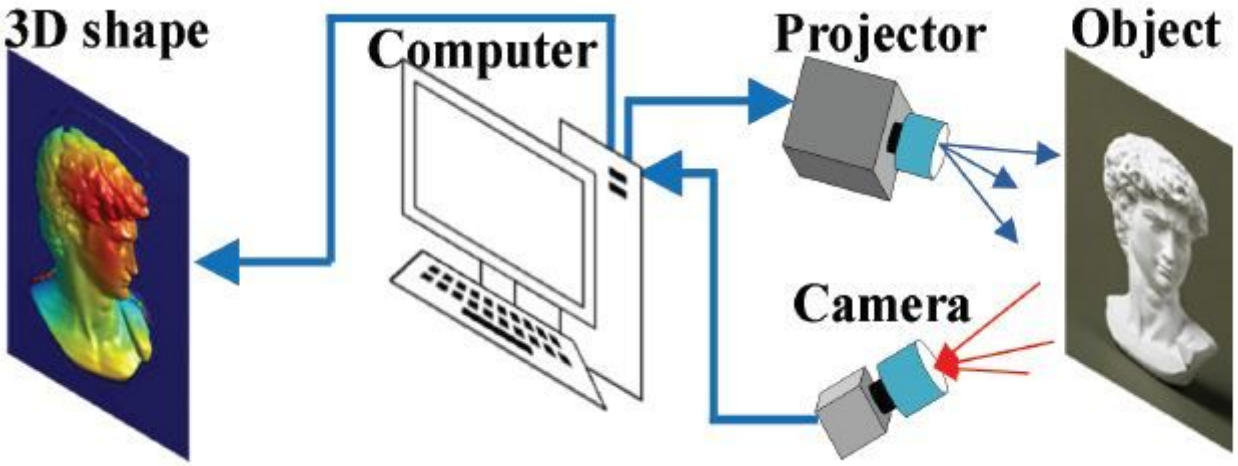

Figure 9

Structure of the 3-D measurement system.

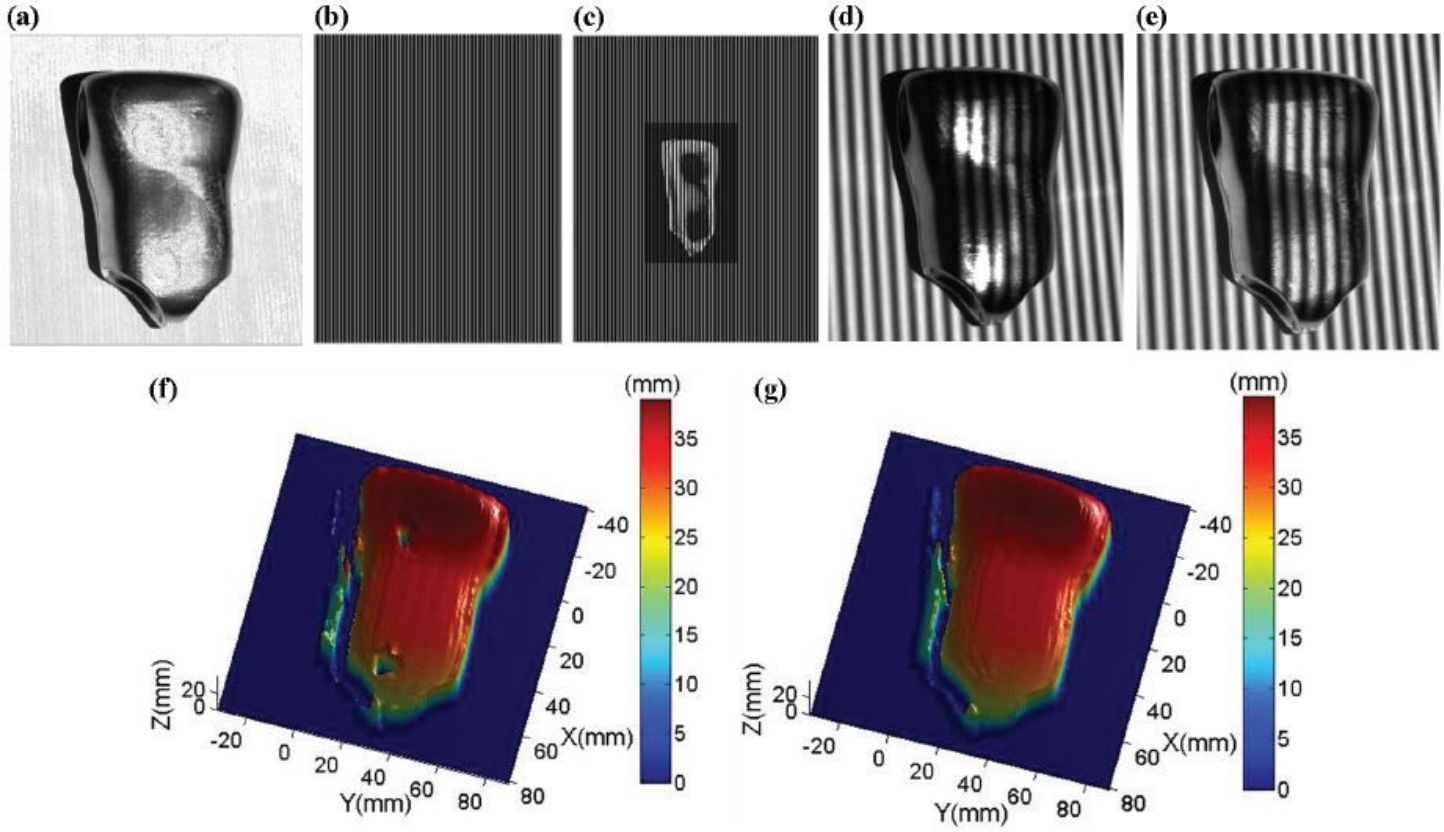

Figure 10

3-D shape reconstruction of a metal product 2. (a) A metal product. (b) Original projection fringe pattern. (c) Optimized projection fringe pattern. (d) Original captured fringe pattern. (e) Optimized captured fringe pattern. (f) Reconstructed 3-D surface shape using the original captured fringe patterns. (g) Reconstructed 3-D surface shape using the optimized captured fringe patterns.

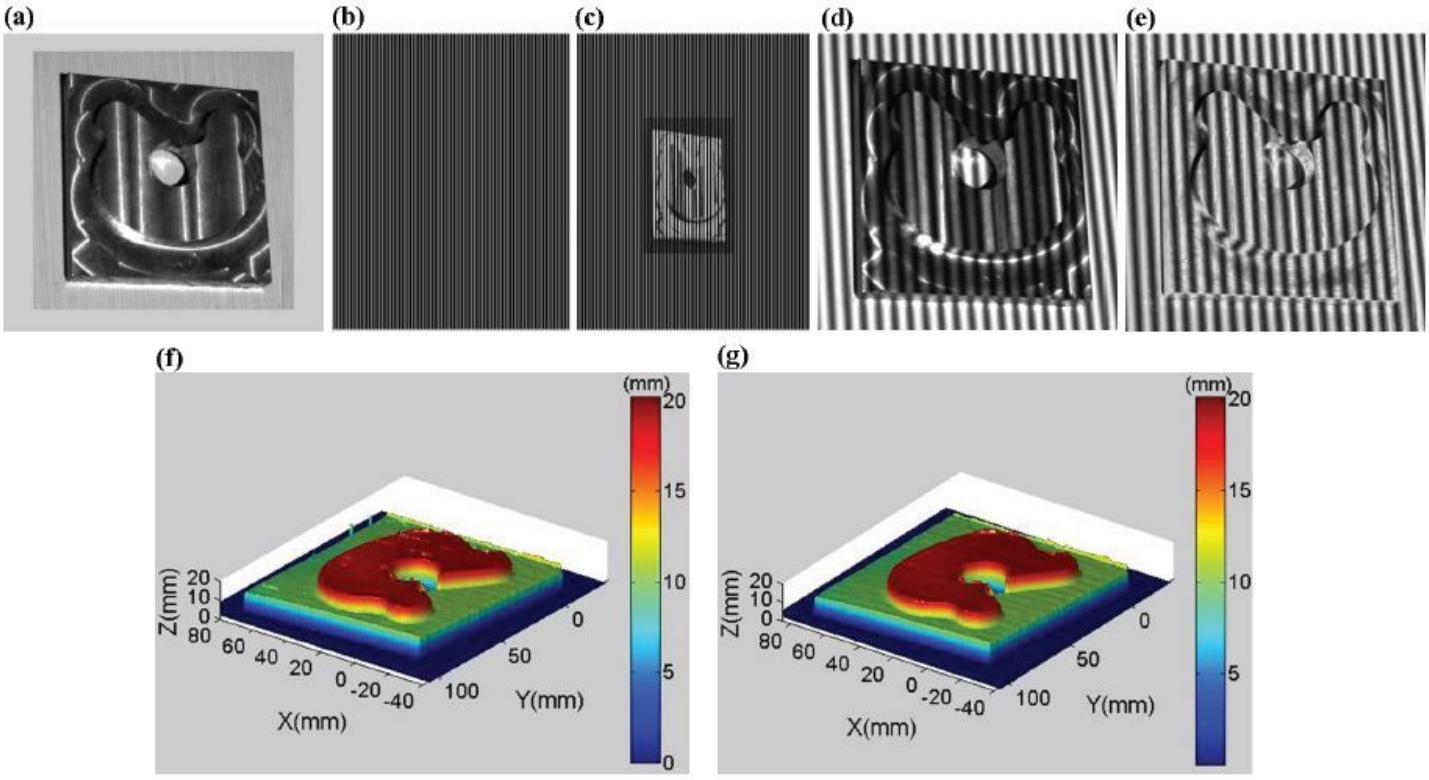

Figure 11

3-D shape reconstruction of another metal product 2. (a) Another metal product. (b) Original projection fringe pattern. (c) Optimized projection fringe pattern. (d) Original captured fringe pattern. (e) Optimized captured fringe pattern. (f) Reconstructed 3-D surface shape using the original captured fringe patterns. (g) Reconstructed 3-D surface shape using the optimized captured fringe patterns.

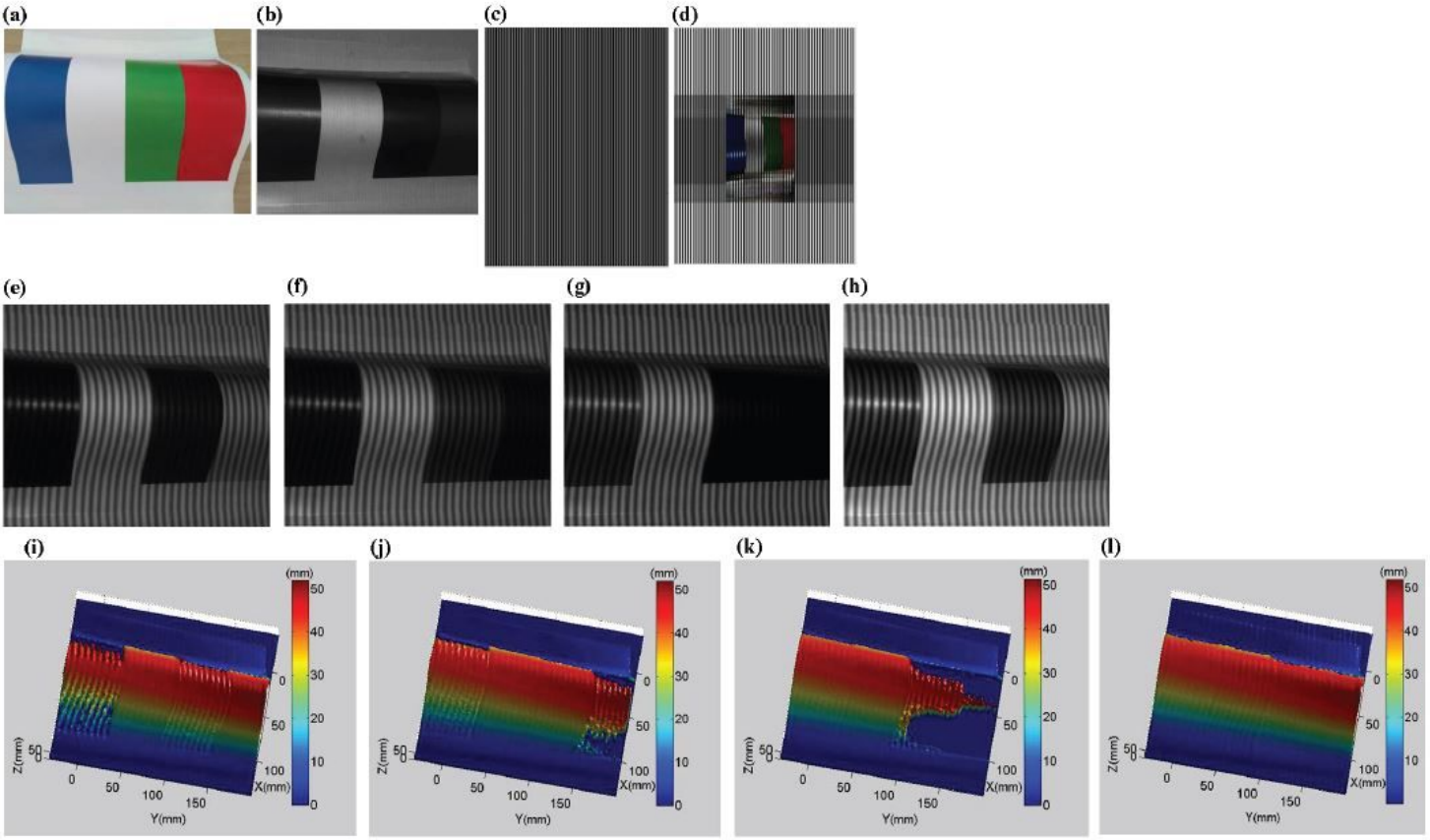

Figure 12

3-D shape reconstruction of a colorful object. (a) A colorful object. (b) A captured image without fringe projection. (c) Original projection fringe pattern. (d) Optimized projection fringe pattern. (e) A captured fringe pattern during red light projection. (f) A captured fringe pattern during green light projection. (g) A captured fringe pattern during blue light projection. (h) Optimized captured fringe pattern using the method proposed in this paper. (i) Reconstructed 3-D surface shape during red light projection. (j) Reconstructed 3-D surface shape during green light projection. (k) Reconstructed 3-D surface shape during blue light projection. (l) Reconstructed 3-D surface shape using the method proposed in this paper.

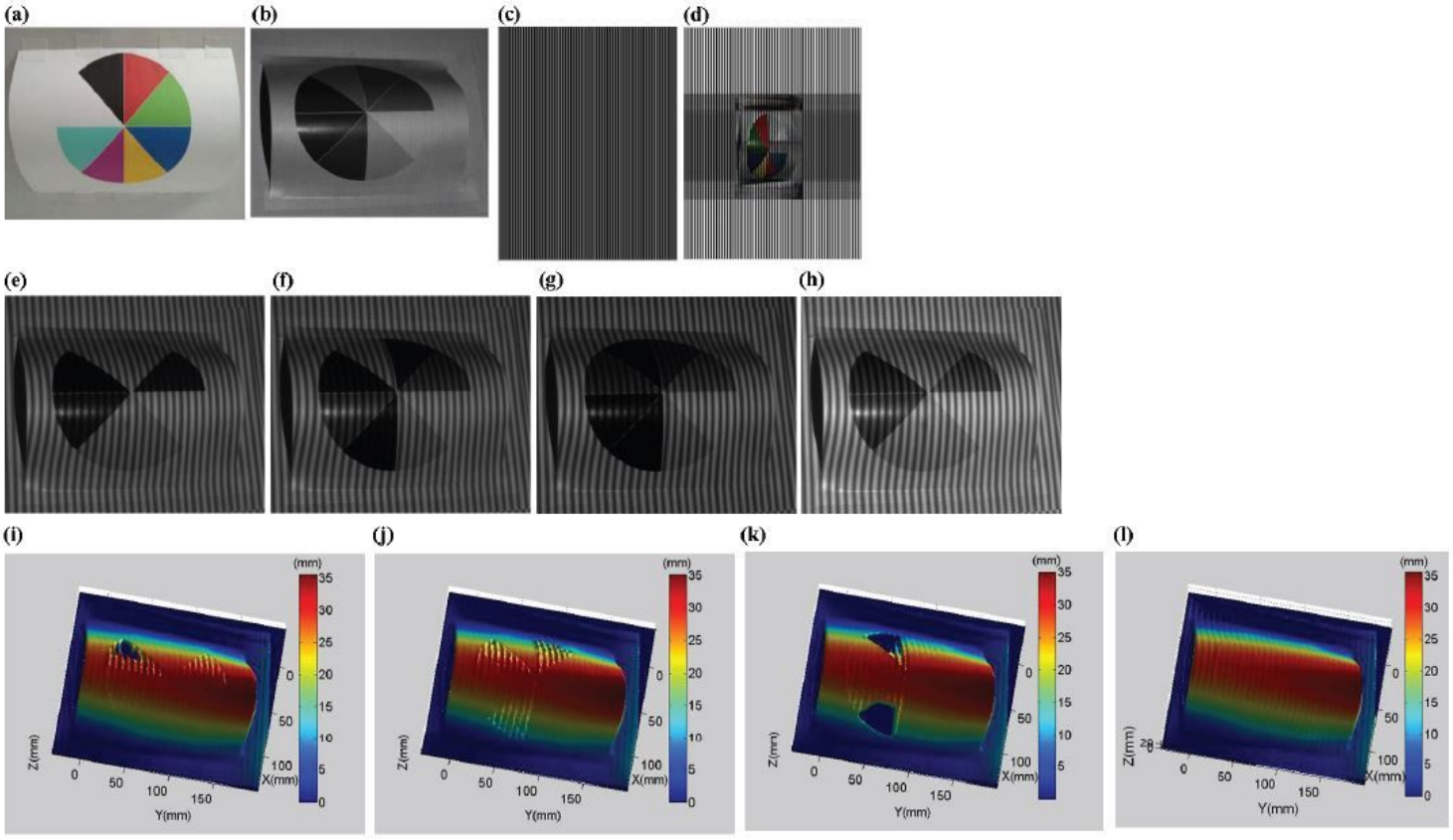

Figure 13

3-D shape reconstruction of a colorful object. (a) Another colorful object. (b) A captured image without fringe projection. (c) Original projection fringe pattern. (d) Optimized projection fringe pattern. (e) A captured fringe pattern during red light projection. (f) A captured fringe pattern during green light projection. (g) A captured fringe pattern during blue light projection. (h) Optimized captured fringe pattern using the method proposed in this paper. (i) Reconstructed 3-D surface shape during red light projection. (j) Reconstructed 3-D surface shape during green light projection. (k) Reconstructed 3-D surface shape during blue light projection. (l) Reconstructed 3-D surface shape using the method proposed in this paper.